ANKARA YILDIRIM BEYAZIT UNIVERSITY

GRADUATE SCHOOL OF NATURAL AND APPLIED SCIENCES



DESIGN AND DEVELOPMENT OF ON-CHIP DEP BASED ANTIBIOTIC PERMEABILITY DEVICE

M.Sc. Thesis by

Jaspreet Kaur

Department of Electrical and Electronic Engineering

June 2019

ANKARA

DESIGN AND DEVELOPMENT OF ON-CHIP DEP BASED ANTIBIOTIC PERMEABILITY DEVICE

A Thesis Submitted to

The Graduate School of Natural and Applied Sciences of

Ankara Yıldırım Beyazıt University

In Partial Fulfillment of the Requirements for the Degree of Master of Science in Electrical and Electronic Engineering, Department of Electrical and Electronic Engineering

by

Jaspreet Kaur

June 2019

ANKARA

M.Sc. THESIS EXAMINATION RESULT FORM

We have read the thesis entitled **"DESIGN AND DEVELOPMENT OF ON-CHIP DEP BASED ANTIBIOTIC PERMEABILITY DEVICE"** completed by **JASPREET KAUR** under the supervision of **ASSIST. PROF. DR. FATMA DOGAN GUZEL** and we certify that in our opinion it is fully adequate, in scope and in quality, as a thesis for the degree of Master of Science.

Assist. Prof. Dr. Fatma DOĞAN GÜZEL

Supervisor

Assoc. Prof. Dr. Mehmet ÜNLÜ

Jury Member

Assist. Prof. Dr. Begum ÜNVEROĞLU

Jury Member

Prof. Dr. Ergün ERASLAN

Director

Graduate School of Natural and Applied Sciences

ETHICAL DECLARATION

I hereby declare that, in this thesis which has been prepared in accordance with the Thesis Writing Manual of Graduate School of Natural and Applied Sciences,

- All data, information, and documents are obtained in the framework of academic and ethical rules,
- All information, documents, and assessments are presented in accordance with scientific ethics and morals,
- All the materials that have been utilized are fully cited and referenced,
- No change has been made on the utilized materials,
- All the works presented are original,

and in any contrary case of the above statements, I accept to renounce all my legal rights.

Date: **2019, 26 June**

Signature: .....

Name & Surname: Jaspreet Kaur

ACKNOWLEDGMENTS

I am sincerely grateful to my advisor Dr. Fatma Dogan Guzel whose guidance, motivation and belief in me have made the journey as a master's student in research interesting and adventurous. Not only do I think she is the ideal supervisor, but she has also been a great mentor. To her, I am forever grateful. My gratitude also goes to the members of the Biomedical Engineering Laboratory at Ankara Yildirim Beyazit University for their useful input and support. I thank Dr. Hamed Ghorbanpoor who became a guide and family member to me, I felt immense pleasure to work with him. His technical skills assisted me to land my roller coaster ride smoothly. I am also thankful to Yasin Ozturk, Iremnur, and Vahit Guzel for their assistance and engineering skills during my project. Dr. Araz Norouz Dizaj is 'the wise one' throughout my learning process, he answered all the questions based on chemistry.

This thesis would not have been possible unless working at the Nano-Micro Engineered and Manufacturing System laboratory at Istanbul Technical University. I would like to extend my gratitude to Prof. Dr. Levent Trabzon and his laboratory team for offering support about experiments. I also owe a thank to Prof. Sinan Kivrak for allowing me to perform the characterization of the device in his Power Electronics Laboratory at AYBU. I am also beholden by Dr. Cihan Darcan and Ozge Kaygusuz for porin production at Bilecik Şeyh Edebali University.

I express my gratitude to AYBU for the unique opportunity of working with world-class professors. I am also indebted to everyone who wishes me well in everything I do whether in person or in secrete. A special thanks goes to my family and friends for their undying love toward me. I thank my mother and father, for believing in me. I am truly blessed and grateful to have them in my life. Above all, I thank God for this wonderful experience called life.

This project was funded by TÜBİTAK under the grant number:217M151.

2019, 26 June **Jaspreet Kaur**

DESIGN AND DEVELOPMENT OF ON-CHIP DEP BASED ANTIBIOTIC PERMEABILITY DEVICE

ABSTRACT

Biosensors have a wide range of applications in different sectors such as food, environment, defense, and most importantly medicine. To increase the ease of fabrication, cost-effectiveness, durability, accuracy and many more other features of these devices, the researchers are still working to make them cheaper, smaller (portable), simple and more sophisticated at the same time. One of the best ways to do so is to develop an integrated lab on chip systems (LOC). LOC biosensors are, in particular, of great importance in medicine because they may provide physicians with a quicker response about the patient situation. LOC biosensors are nowadays designed to compose of Polydimethylsiloxane (PDMS)-based microfluidic networks and could be integrated with other sensor platforms to make the analysis more efficient in terms of cost, time and throughput. In this study, an integrated LOC biosensor comprising of a microelectrode chip and (PDMS)-based microfluidic chip has been developed for the rapid detection of permeability of antibiotics through the artificial cell walls, which represent the bacteria cell wall. This chip enables us to recognize the permeability of antibiotics into the artificial cells based on an electrochemical measurement. Because the detection is electrochemical, there is not any need for labeling of the molecules and also non-fluorescent antibiotics can also be studied, as opposed to the reports published earlier [7, 9]. Giant unilamellar lipid vesicles containing 1,2-diphytanoyl-sn-glycero-3-phosphocholine (DPHPC) lipids have been generated to act as model cell. Electrochemical measurements are performed by an LCR meter which infers the relationship between signal versus time. The measured signal recorded from the chip has been used to determine the change in concentration inside and outside the model bio particles. The whole chip size is approximately 38*26 mm which is quite easy to handle, overall cheap to make and sensitive.

Keywords: Dielectrophoresis, lab-on-a-chip, micro-fabrication, microfluidics, impedance measurement, giant unilamellar vesicles, electroformation.

ÇİP ÜZERİNE DİELEKTROFOREZ DAYALI ANTİBİYOTİK GEÇİRGENLİK CİHAZININ TASARIMI VE GELİŞTİRİLMESİ

ÖZ

Biyosensörlerin alanın uygulamaları oldukça geniştirç Örnek olarak gıda, çevre, savunma ve daha önemlisi tıp gibi çeşitli sektörlerde kullanılmaktadırlar. Fabrikasyon kolaylığını, maliyet etkinliğini, dayanıklılığı, doğruluğu ayrıca cihazların birçok özelliğini arttırmak nedeniyle araştırmacılar hala da onları daha uygun ve ucuz, daha küçük (kolay taşınabilir), aynı anda daha basit ve daha sofistike hale getirmek için araştırmalar devam etmektedir. Bunu yapabilmek için en iyi yollarından biri çip üzerine entegre laboratuvar sistemlerin (LOC) geliştirilmesidir. LOC biyosensörleri özellikle tıpta büyük öneme sahiptiler çünkü doktora hasta durumu hakkında daha hızlı yanıt verebilirler. LOC biyosensörleri günümüzde PDMS tabanlı mikro-akışkan ağları oluşturmak için tasarlanmıştır. Ayrıca maliyet, zaman ve verim açısından analizi daha verimli hale getirmek için diğer sensör platformlarıyla entegre edilebilir. Bu çalışmada, bakteri hücre duvarını temsil eden yapay hücre duvarları yoluyla antibiyotik geçirgenliğinin hızlı bir şekilde tespit edilmesi için tasarlanmış bir mikro-elektrot çipi ve mikro-akışkan çipten oluşan LOC entegre bir biyosensörü geliştirilmiştir. Böylece çip, bir elektrokimyasal ölçüme dayanarak antibiyotiklerin yapay hücrelerden geçirgenliğini tanımamızı sağlar. Hazırlanan çip algılama elektrokimyasal olduğu için, moleküllerin etiketlenmesine gerek yoktur ayrıca daha önce yayınlanan raporların aksine floresan olmayan antibiyotikler de incelenebilir. Çalışmamızda, 1,2-diftanoil-sn-gliserol-3-fosfokolin (DPHPC) lipidlerini içeren dev unilamellar lipit vezikülleri (GUVs), model hücre olarak görev yapmak için hazırlanımıştır. Elektrokimyasal sinyal ölçümü, sinyal ve zaman arasındaki ilişkiyi etkileyen bir LCR metre ile gerçekleştirilir. Çipten kaydedilen ölçülen sinyal, biopartikül modelinin içindeki ve dışındaki konsantrasyon değişimi LCR metre belirleyebilir. Çipin büyüklüğü yaklaşık 38 * 26 mm'dir ve kullanımı oldukça kolaydır, genel olarak yapımı ucuz ve hassastır.

Anahtar Kelimeler: Dielektroforez, çipte laboratuar, mikro imalat, mikroakışkanlar, empedans ölçümü, dev unilamel veziküller, elektroformasyon.

CONTENTS

M.Sc. THESIS EXAMINATION RESULT FORM ii
ETHICAL DECLARATION iii
ACKNOWLEDGMENTS iv
ABSTRACT v
ÖZ vi
LIST OF TABLES xi
LIST OF FIGURES xii

CHAPTER 1- INTRODUCTION 1
1.1 Literature Review 1
1.2 Motivation 1
1.3 Lab on chip (LOC) 3
1.4 MEMS - Microelectromechanical systems 4
1.5 Biosensor 6
1.6 Microfluidics 10
1.7 Dielectrophoresis 13
1.8 Giant Unilamellar Vesicles 16
1.9 Antibiotic Permeability 19
1.9.1 Antibiotics 19
1.9.2 Permeability 20
1.10 Summary 21
CHAPTER 2-PREPARATION OF GIANT UNILAMELLAR VESICLES 22
2.1 Materials 22
2.2 Preparation of Aqueous solutions: 23
2.3 Production of GUVs. 23
2.3.1 Preparation of phospholipid stock solution 23
2.3.2 Electroformation 23
2.3.3 OmpF Incubation to Vesicles 25
2.4 Summary 25
CHAPTER 3- CHIP FABRICATION 26
3.1 Fabrication of Chip 1 26
3.1.1 Production of Electrode Array 26

3.1.2 Production of Microfluidic chip 29
3.1.3 Assembly 29
3.2 Fabrication of Chip 2 30
3.2.1 Designing of Microfluidic Chips 30
3.2.2 Production of Electrode Array 31
3.2.3 Production of Microfluidic Channels 35
3.2.4 Integration of Microfluidic chip onto Electrode chip 39
3.3 Summary 40
CHAPTER 4- EXPERIMENTAL APPROACH 41
4.1 Off-chip Experiments 42
4.1.1 Conductivity Measurements: 42
4.1.2 Impedance Measurements: 42
4.2 On-chip Experiments 42
4.2.1 Impedance Measurements: 44
4.3 Summary 44
CHAPTER 5- RESULTS AND DISCUSSION 45
5.1 Giant Unilamellar Vesicle 45
5.1.1 Gaussian Distribution 45
5.2 Permeability Testing 52
5.3 Off-chip passive permeability testing 52
5.3.1 Conductivity Measurements 53
5.3.2 Impedance Measurements 54
5.4 Off-chip active permeability testing 54
5.4.1 Conductivity Measurements 55
5.4.2 Impedance Measurements 55
5.5 Comparison of Off-chip Passive and Active Permeability Testing 56
5.6 On-chip Passive Permeability Testing 58
5.6.1 Impedance Measurements 58
5.7 On-chip active permeability testing 58
5.7.1 Impedance Measurements 59
5.8 Comparison of On-chip Passive and Active Permeability Testing 59
5.9 Discussion 61
CHAPTER 6- CONCLUSION 65
REFERENCES 66

CURRICULUM VITAE 70

ABBREVIATIONS

GUVs	Giant Unilamellar Vesicles
Pro-GUVs	Protein embedded Giant Unilamellar Vesicles
NF	Norfloxacin
DEP	Dielctrophoresis
AC-DEP	Alternating Current Dielctrophoresis
PDMS	Polydimethylsiloxane
MEMS	Microelectronic Mechanical Systems
LOC	Lab-On-chip
UCOF	Upper Crossover Frequency
UV	Ultraviolet
PR	Photoresist
PMMA	Polymethylmethacrylate
DPhPC	1,2-diphytanoyl-sn-glycerol-3-phosphocholine
OPOE	Octyl-polyoxyethylene
TRIS	Tris(hydroxymethyl)aminomethane
ITO	Indium tin oxide
OmpF	Outer membrane porin F

LIST OF TABLES

Table 1.1 The development of biosensors since its invention 8

Table 1.2 Summarizes different sensing techniques with their advantages and disadvantages for the detection of a range of analytes using the most common transducers 9

Table 1.3 The table compares the different types of microfluidics with their pros and cons 11

Table 1.4 Advantages and disadvantage of using different fabrication methods and materials for fabricating microfluidic devices for biosensing applications 12

Table 1.5 Comparison of Costs, Advantages, and Disadvantages of different materials during Electroformation 19

Table 2.1 The parameter of Electroformation method 24

Table 4.1 Experimentation Methods 41

Table 4.2 Ways of antibiotic transport to GUVs 41

Table 4.3 Time calculation for given flow rate 43

Table 5.1 The table shows the percentage of GUVs under and above 30-um generated after keeping for 5 minutes in a desiccator 47

Table 5.2 The table shows the percentage of GUVs under and above 30-um generated after keeping for 10 minutes in a desiccator 48

Table 5.3 The table shows the percentage of GUVs under and above 30-um generated after keeping for 15 minutes in a desiccator 49

Table 5.4 The table shows the percentage of GUVs under and above 30-um generated after keeping for 20 minutes in a desiccator 50

Table 5.5 The table shows the percentage of GUVs under and above 30-um generated after keeping for 25 minutes in a desiccator 51

Table 5.6 The table shows the percentage of GUVs under and above 30-um generated after keeping for 30 minutes in a desiccator 52

LIST OF FIGURES

Figure 1.1 Schematic of Device 2

Figure 1.2 Interdisciplinary fields of LOC 3

Figure 1.3 Classification of microsystem technology 4

Figure 1.4 MEMS devices 5

Figure 1.5 BioMEMS market forecast by Yole Développement 6

Figure 1.6 Bio-MEMS applications 6

Figure 1.7 Schematic representation of biosensor 7

Figure 1.8 Schematic of types of different microfluidic (a) continuous; (b) drop-based; (c) digital 10

Figure 1.9 DEP force on induced dipoles with a non-uniform electric field 14

Figure 1.10 DEP spectrum (Re[K(ω)] vs. frequency) of a polarizable particle. 16

Figure 1.11 Schematic of unilamellar vesicles and their size distribution 17

Figure 1.12 Schematic of electroformation and optical image of GUVs 18

Figure 1.13 Structure of Norfloxacin 20

Figure 1.14 Transportation of particles through the membrane is passive permeability and via membrane containing porins is active permeability 20

Figure 2.1 Required materials and set up for generating GUVs 22

Figure 2.2 Protocol for Electroformation technique 24

Figure 3.1 Electrode spacing accuracy 27

Figure 3.2 Finished view of lab-on-chip 30

Figure 3.3 2D and 3D view of the main parts of a microfluidic chip 31

Figure 3.4 Velocity profile of the microfluidic channel 31

Figure 3.5 Flow diagram of fabrication (schematic and practical) 32

Figure 3.6 Photo Mask of the electrode 32

Figure 3.7 Setup of spin coating and baking 33

Figure 3.8 The photomask of the electrode is placed on PR coated glass slide 34

Figure 3.9 The pasted photomask of the electrode over PR coated glass slide rested under the in-house developed UV light source 34

Figure 3.10 sputtering process 35

Figure 3.11 Flow diagram of fabrication..... 36

Figure 3.12 Photomask of the microfluidic channel 36

Figure 3.13 Setup of spin coating and baking 37

Figure 3.14 Fabricated template on a silicon wafer 38

Figure 3.15 Steps to be followed to get the microfluidic chips..... 39

Figure 3.16 Cutting out the area containing microchannel 39

Figure 3.17 Manual alignment 40

Figure 3.18 Epoxy Bonding 40

Figure 4.1 Conductivity Test Setup and Test equipment of impedance measurement 42

Figure 4.2 Entire set up 43

Figure 5.1 The image of GUVs generated by Electroformation was taken by an optical microscope at magnification 40X. Scale bar is 10um 45

Figure 5.2 Comparison between the mean value of all size of GUVs and GUVs under the 30-um generated after keeping for 5 minutes in a desiccator..... 46

Figure 5.3 Comparison between the mean value of all size of GUVs and GUVs under the 30-um generated after keeping for 10 minutes in a desiccator..... 47

Figure 5.4 Comparison between the mean value of all size of GUVs and GUVs under the 30-um generated after keeping for 15 minutes in a desiccator..... 48

Figure 5.5 Comparison between the mean value of all size of GUVs and GUVs under the 30-um generated after keeping for 20 minutes in a desiccator..... 49

Figure 5.6 Comparison between the mean value of all size of GUVs and GUVs under the 30-um generated after keeping for 25 minutes in a desiccator..... 50

Figure 5.7 Comparison between the mean value of all size of GUVs and GUVs under the 30-um generated after keeping for 30 minutes in a desiccator..... 51

Figure 5.8 Impedance measurement with respect to the frequency range 53

Figure 5.9 conductivity versus time 53

Figure 5.10 Impedance and admittance shifts over time of NF loaded GUVs. 54

Figure 5.11 Conductivity versus time 55

Figure 5.12 Impedance and admittance shifts over time of NF loaded pro-GUVs... 56

Figure 5.13 The comparison between the impedance and admittance shift of NF (pH-5) loaded GUVs and pro-GUVs 57

Figure 5.14 The comparison between the impedance and admittance shift of NF (pH-7) loaded GUVs and pro-GUVs 57

Figure 5.15 The comparison between the impedance and admittance shift of NF (pH-9) loaded GUVs and pro-GUVs 57

Figure 5.16 Impedance and admittance shifts over time of NF loaded GUVs 58

Figure 5.17 Impedance and admittance shifts over time of NF loaded pro-GUVs... 59

Figure 5.18 The comparison between the impedance and admittance shift of NF (pH-5) loaded GUVs and pro-GUVs 60

Figure 5.19 The comparison between the impedance and admittance shift of NF (pH-7) loaded GUVs and pro-GUVs 60

Figure 5.20 The comparison between the impedance and admittance shift of NF (pH-9) loaded GUVs and pro-GUVs 61

Figure 5.21 Electric model of membrane 62

CHAPTER 1

INTRODUCTION

1.1 Literature Review

Dielectrophoresis (DEP) is a phenomenon in which a force is exerted on a dielectric particle when it is subjected to a non-uniform electric field. It was discovered by Pohl et al who explained the usage of non-uniformity of the potential difference [14] His revolutionary research became a ground for future work. His work was constrained to modulate the micron size particles but in the 1990s, N G Green et al [17] disapproved his thoughts when sub-micron particles were successfully captured using DEP. After the publication of Jones's book on Electromechanics of Particles [20], the detailed mathematics behind the DEP force was explained. However his work did not depict the relation of DEP forces on submicron particles. Researchers like Castellanos, Ramos, Gonzalez, Green, and Morgan [13] dealt with scaling law afterwards. To validate the DEP effect on submicron sized bioparticles, Gerard et al [24] represented the mobility of bioparticles under the effect of positive DEP because of continuously increment in conductivity of aqueous solution flowing in the channel. The bioparticles act as such particles which possess dielectric properties and because of dielectric properties, particles releases from the channel at a specific flow rate. Moreover, an investigation on the biophysical properties of the enveloped mammalian virus, has also been performed by Michael et al [19]. The smeared-outshell model has been used to determine the dielectric properties of viruses under DEP response. Similarly, Alexander et al [26] determined the dielectric constant (ε) and electrical conductivity (σ) of the PS particles not with DEP but with an LCR meter from a lower frequency to the high-frequency range.

1.2 Motivation

In the past, a patient was treated without any proper diagnosis. Albeit, in present, with the help of miniaturization and portability of devices, any ailment can be detected

before it happens. Lab on chip technology has made a crucial impact on global health particularly with the integration of dielectrophoresis and microfluidics that do wonders in medical/bioscience. In dielectrophoresis, with the application of non-uniform alternating or direct electric field, the bioparticles of different polarity becomes easily distinguishable. In addition, microfluidic systems have gone through recent developments to perform complex and time-consuming biological functions on Lab-on-chip devices. These chips are cost-effective, consume small fluid volume, automated and provide accurate results in a shorter time. These points are considered as advantages of microfluidic devices. Apparently, these systems are used for multiple applications. One of the major sectors is health¸ where prescribing an antibiotic for curing diseases has become sophisticated because Antimicrobial Resistance (AMR) comes into play. Most of the antibiotics have already been tested for Gram-Negative Bacteria (GNB) as it is present everywhere on earth. Treating GNB is a difficult one because of an outer membrane that protects them from antibiotics [3,10–15]. Therefore, the motive of our device is to check the antibiotic permeability rates with the integrated circuitry and indeed, the developed chip will be performing diagnostic tests with no laboratory support. Undoubtedly, MEMS (microelectromechanical systems) has overtaken the entire industrial areas due to its ease of miniaturization, durability, cost-effectiveness, high throughput and for many other features in devices [21].

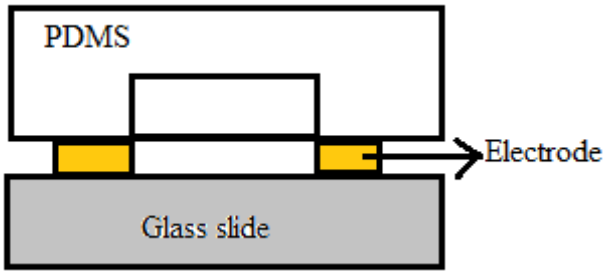

Figure 1.1 Schematic of Device

Eventually, the concept of dielectrophoresis was used to develop the LOC-based antibiotic permeability assay in connection with basic science such as physics, biology, and chemistry. Moreover, dielectrophoresis dispenses the fluorescent requirement for antibiotic permeability measurement, which enables the analysis without any carrier,

and the generated results would be as considerable as the studies performed with fluorescent-based measurements [10]. Figure 1.1 is the expected chip design. In the following sections, relevant terminologies, technologies and concepts are examined in order to understand the basics of this study.

1.3 Lab on chip (LOC)

LOC technology implies the techniques that perform varied laboratory operations on a miniaturized scale like chemical synthesis and analysis on one chip resulting in a hand-held and moveable device. In other words, LOC is a device which is capable of scaling the single or multiple laboratory functions down to a chip-format. The size of the chip ranges from millimeters to a few square centimeters [18]. Figure 1.2 displays the interdisciplinary fields of LOC. The interdisciplinary fields are biosensor, microfluidics, biotechnology, microelectromechanical and nanoelectromechanical systems, very large scale integration.

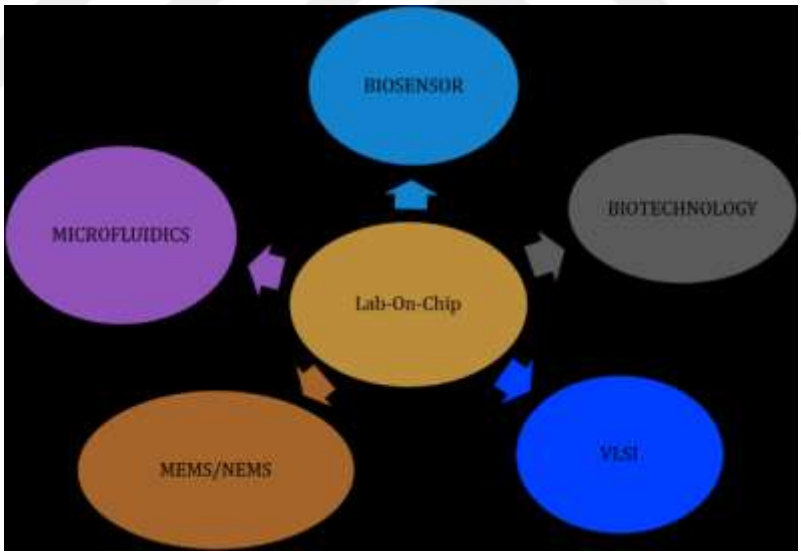

Figure 1.2 Interdisciplinary fields of LOC [42]

LOC devices are often indicated by μTAS (Micro Total Analysis Systems) and a subset of Micro-electromechanical systems (MEMS) devices. LOC technology is closely related to the microfluidics which is primarily the combination of physics, the study, and manipulation of small quantities of fluids.

1.4 MEMS - Microelectromechanical systems

Microelectromechanical systems permit the expansion of electromechanical structures. MEMS integrate mechanical parts, sensors, actuators, and electronics on a silicon substrate using a process technology called microfabrication [31].

These systems are classified as shown in Figure 1.3 such as meechinal, optical, electrical, and also according to physical , chemical and biological areas.

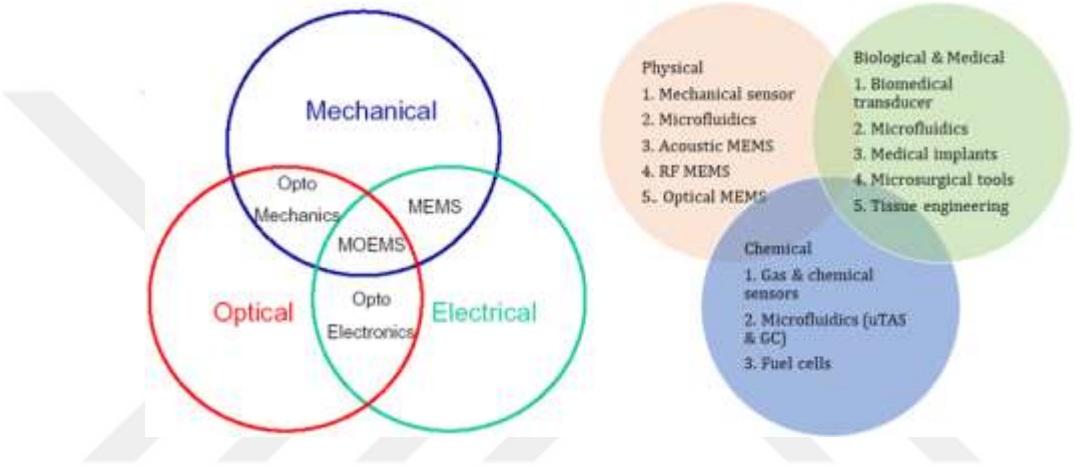

Figure 1.3 Classification of microsystem technology [21, 42]

These systems can do multitasks at a time such as sensing, controlling and activating especially on the micron scale, and functionalize individually or in arrays to generate effects on the macro scale. It integrates typical semiconductor electronics with a number of other electronic devices, at micron level that forms the basis of microelectronics. MEMS technologies make devices ranging from millimeters to microns. Figure 1.4 elaborates the different MEMS devices such as inkjet printer, pressure sensor with integrated circuit (IC) integration, digital mirror device, optical switches and many more.

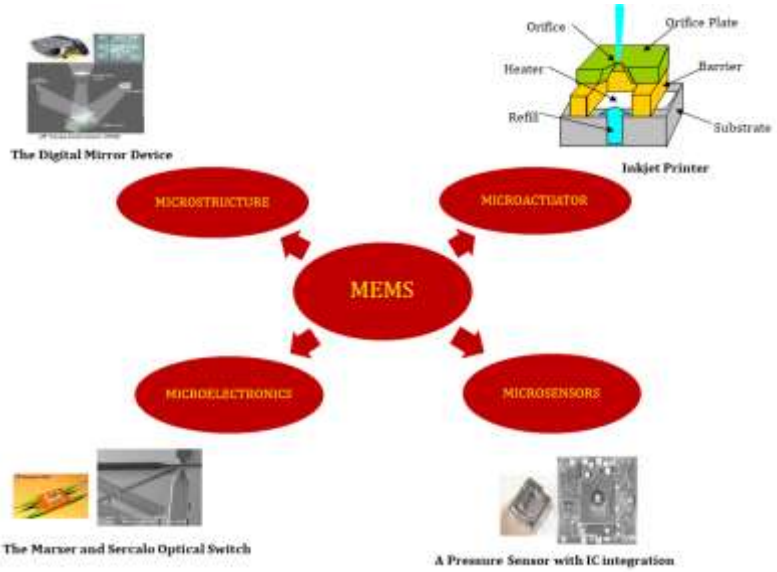

Figure 1.4 MEMS devices [21]

Another evergrowing field of MEMS falls under the biomedical category, generally known as BioMEMS. BioMEMS application areas include transducers for medical use, microsurgical tools, microfluidics, medical implants, and tissue engineering. In the Biomedical field, MEMS have advantages in the medical area for

- The Biomedical Instruments and Analysis.
- Implants and Drug Delivery.

There are some reasons for the necessity of miniaturization like:

- Cost reduction
- Less intrusive surgical procedures
- Health concerns
- A small volume of test sample needed, picolitres
- Quick diagnosis
- Patient recovery time
- Ease of usage

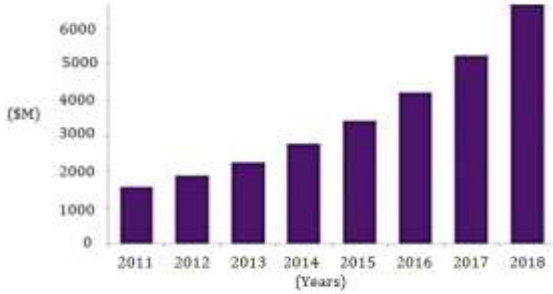

Figure 1.5 BioMEMS market forecast by Yole Développement [43]

And Figure 1.5 displays the increment in the trend of BioMEMS in market forecasted by Yole Développement [43]. Moreover, other BioMEMS applications include tissue engineering and microfluidics for cell biology, proteomics, and genomics (Figure 1.6).

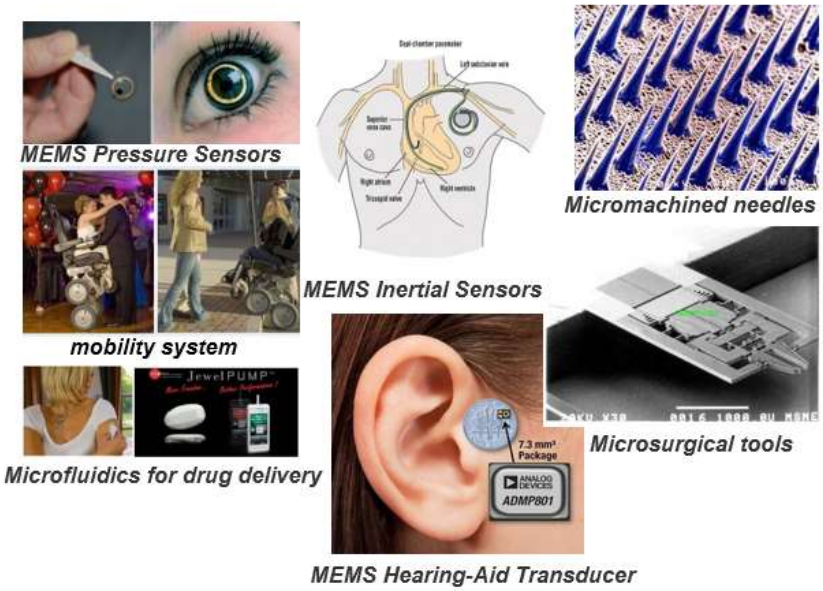

Figure 1.6 Bio-MEMS applications [36]

In the next section, biosensors will be examined in the context of BioMEMS devices.

1.5 Biosensor

A biosensor is defined as a sensor that integrates a biological element with a physiochemical transducer to produce an electronic signal proportional to a single

analyte which is then conveyed to a detector. Figure 1.7 shows the schematic representation of biosensor [23]. The figure explains the stages of analyzing the bioparticles in the form of quantifiable unit. A biosensor takes biological elements then with transducer, the response is measured and monitored after signal amplification and processing.

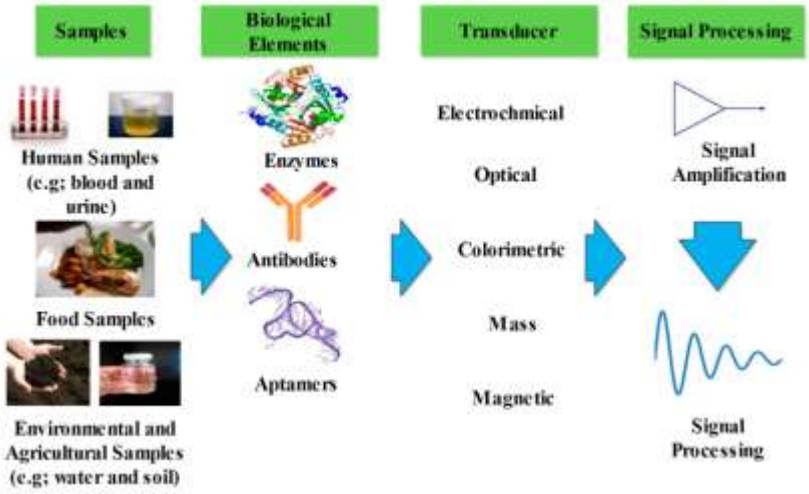

Figure 1.7 Schematic representation of biosensor [4]

History of Biosensors

The history of biosensors begins in 1916 when proteins were immobilized on activated charcoal for the first time. Then, the concept of pH (hydrogen ion concentration) was introduced by Søren Peder Lauritz Sørensen and an electrode for pH measurements was realized in the year 1922 by W.S. Hughes. However, the first 'true' biosensor was developed for oxygen detection by Leland C. Clark, Jr in 1956. His invention of the oxygen electrode bears his name: 'Clark electrode' and he has then been recognized as the father of sensors. Later in 1962, he demonstrated an amperometric enzyme electrode for the detection of glucose and this was followed by the first potentiometric biosensor to detect urea by Guilbault and Montalvo in 1969. Eventually, in 1975, the first commercial biosensor was developed by Yellow Spring Instruments (YSI). Table 1.1 shows the historical overview of biosensors in the period 1970–1992. The field is now a multidisciplinary area of research that bridges the principles of basic sciences (physics, chemistry, and biology) with fundamentals of micro/nano-technology, electronics and applicatory medicine [23].

Table 1.1 The development of biosensors since its invention [22]

1916	First report on immobilization of proteins: adsorption of invertase on activated charcoal
1922	First glass pH electrode
1956	Clark published his definitive paper on the oxygen electrode.
1962	First description of a biosensor: an amperometric enzyme electrode for glucose (Clark)
1975	First commercial biosensor (YellowSprings Instruments glucose biosensor)
1975	First microbe-based biosensor, First immunosensor
1976	First bedside artificial pancreas (Miles)
1998	Blood glucose biosensor launch by LifeScan FastTake
1998	Roche Diagnostics by Merger of Roche and Boehringer Mannheim
Now	Quantum dots, nanoparticles, nanowire, nanotube, etc

Basic characterization of Biosensor

Four parameters are considered to be the very important characterization of biosensors.

Linearity: Linearity of the sensor should be high for the detection of high substrate concentration.

Sensitivity: Value of the electrode response per substrate concentration.

Selectivity: Chemicals Interference must be minimized for obtaining the correct result.

Response time: Time necessary for having 95% of the response.

Types of Biosensors

The two important parts that distinguish the biosensors are

- Type of biological recognition sensing element
- Transducers.

Table 1.2 Summarizes different sensing techniques with their advantages and disadvantages for the detection of a range of analytes using the most common transducers [23]

Transducer	Technique	Advantages	Disadvantages
Electrochemical	Amperometric	Simplicity, miniaturization, low cost	Need redox elements to enhance the current production; time-consuming; sensitive to the surrounding environment
	Potentiometric	Real-time detection; the possibility of continuous analysis on different analytes	Sensitive to the surrounding environment; time-consuming; sensitive to temperature
	Impedimetric	Simplicity and real-time detection Real-time	Sensitive to the surrounding environment; bulky devices required; require theoretical stimulation for data analysis
Optical	Surface plasmon resonance	Real-time detection; reliable, high sensitivity Real-time	Sensitive to the surrounding environment; surface modification as one of the main challenges; bulky optical devices required
Mechanical	cantilever	Real-time detection; ability to detect more than one analyte with high sensitivity	Sensitive to the surrounding environment; sensitive to temperature; bulky devices required

With this perspective, Table 1.2 summarizes the advantages and disadvantages of the detection of a range of analytes using the most common transducers using different sensing techniques [23].

The following section will describe another field of LOC that is microfluidics in detail. The details will include types of microfluidics, advantages, and disadvantages of different types of microfluidics, fabrication and its application.

1.6 Microfluidics

Microfluidics is a branch which studies the behavior of fluids through microchannels, and the technology of manufacturing microminiaturized devices containing chambers and tunnels through which fluids flow. Microfluidics deal with very small volumes of fluids, down to femtoliters (fL). Fluids behave very differently on the micrometric scale than they do in everyday life. These unique features are the key to new scientific experiments and innovations.

Microfluidics falls under three categories.

- Continuous-flow Microfluidics
- Droplet-Based Microfluidics
- Digital Microfluidics

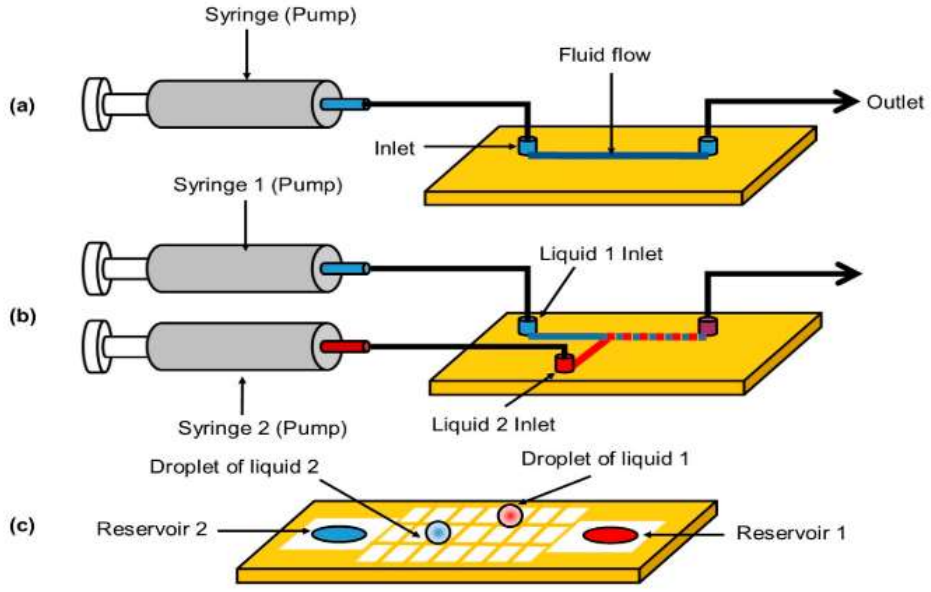

Figure 1.8 Schematic of types of different microfluidic (a) continuous; (b) drop-based; (c) digital [23]

Table 1.3 The table compares the different types of microfluidics with their pros and cons [23]

	Continuous-Flow Microfluidics	Droplet-Based Microfluidics	Digital Microfluidics
Flow Actuation	Mechanical (syringe) pumps, Pneumatic pressure, Electrokinetic Ease	The motion of droplets in micro-channels using streams of immiscible fluids	The motion of discrete droplets on an array of planar electrodes
Flow Actuation	Mechanical (syringe) pumps, Pneumatic pressure, Electrokinetic	Mechanical (syringe) pumps, Dielectric, Pneumatic pressure	Electrowetting On Dielectric, Dielectrophoresis
Advantages	Ease of fabrication and operation, suitable for applications that require a continuous flow with relatively high sampling volume, and is compatible with most of the current screening and sensing mechanisms	Ease of fabrication and operation, suitable for applications that require isolated reaction sites to avoid cross-contamination	Lower sample consumption, scalability, better localization, isolated reaction reconfigurability, and portability
Disadvantages	High sample volume consumption compared to other microfluidic systems, possible contamination, and not being scalable due	No control over individual droplets, challenging to create droplets of different sizes using the same setup, and challenging to	Complicated fabrication procedure, and bio-adsorption and evaporation

Figure 1.8 shows the schematic of types of different microfluidic (a) continuous: these conventional microfluidic systems are based on the continuous flow regimes in micron-sized channels; (b) drop-based: droplet-based microfluidic systems utilized the continuous stream of two or more fluid mainly intersected at a T-junction to create

discrete droplets which are isolated from each other using an immiscible fluid; (c) digital: to further decrease the volume consumption [23]. Table 1.3 summarizes the operating and actuation methods, advantages and disadvantages of the three different types of microfluidics [23].

Table 1.4 Advantages and disadvantage of using different fabrication methods and materials for fabricating microfluidic devices for biosensing applications [23]

Fabrication Method	Fabrication Material	Advantages	Disadvantages
Photolithography	PDMS	Portability Cost-effective and high automation High sensitivity	Low throughput Requiring
Soft lithography	PDMS	Real-time detection Portable Disposable Cost-effective	Requiring high sample concentration
Nano-imprinting	PMMA	Cost-effective High sensitivity	Expensive Low throughput

Microfluidic devices are mainly fabricated by considering some features such as the method to improve the biocompatibility, dimensions, and materials. Glass and silicon have been used in the design and fabrication of microfluidic platforms before the benefits of polymethylmethacrylate (PMMA), and polydimethylsiloxane (PDMS)) have been realized in the field. The benefits include low cost, fast turnaround, multiplexed point-of-care diagnostic devices. Table 1.4 summarizes the different fabrication methods and materials used to fabricate microfluidic devices for biosensing applications.

Microfluidics technology has enormous applications in different fields, mainly: [12]

- The biomedical field that allows performing many medical tests on a single chip,
- Cell biology research that allows easy manipulations of single cells,

- Protein crystallization that permits the generation of a large number of crystallization conditions on a single chip (e.g. Temperature, pH, humidity)
- Drug screening,
- Glucose tests,
- Chemical micro-reactor,
- Electrochemistry,
- Microprocessor cooling
- Micro fuel cells.

In short, the microfluidic chip is a pattern of microchannels, molded or engraved. This network of microchannels incorporated into the microfluidic chip is linked to the macro-environment by several holes of different dimensions hollowed out through the chip. It is through these pathways that fluids are injected into and evacuated from the microfluidic chip. Fluids are directed, mixed, separated or manipulated to attain multiplexing, automation, and high-throughput systems. The microchannels network design must be precisely elaborated to achieve the desired features such as lab-on-a-chip, detection of pathogens, Dielectrophoresis, etc.) [25].

The dielectrophoresis will be demonstrated in brief in a further section.

1.7 Dielectrophoresis

One can study the movement of a particle in a microfluidic system in order to trap and sort cells and particles using the active technique, such as dielectrophoresis (DEP) only if the particle is introduced in a non-uniform electric field in the microchannel. Microfluidic chip's favorable scaling for the reduced size of the system is an add on to any application. DEP based microfluidic systems have been utilized for many applications [14].

Besides the other types, in AC-DEP asymmetric array of metal electrodes are embedded in a microfluidic device to generate a non-uniform electric field. AC-DEP separates (bio) particles based on their electrical property and/or size. When the particle has higher polarizability than that of the medium, the net force pushes the

particle towards a small electrode (direction of the maximum electric field) which is known as positive DEP (p-DEP). For the case where the medium has higher polarizability than that of the particle, the net force repels the particles towards the large electrode (direction of minimum electric field strength) which is known as negative DEP (n-DEP) [38]. Schematic sketched can be seen in Figure 1.9. The concept dielectrophoresis has derived from electrophoresis which is explained below.

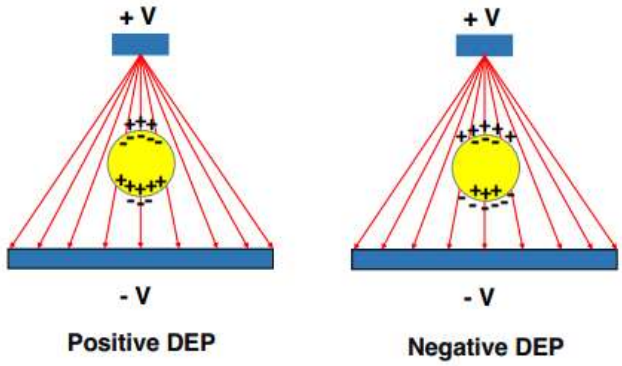

Figure 1.9 DEP force on induced dipoles with a non-uniform electric field [41]

Generally, a particle's dipole has mainly two origins. The first is the permanent dipole which is due to the orientation of the atoms, and it inherently exists. The second is the induced dipole which is due to the reorientation of the charges on the particle's surface with the presence of the external electric field [14].

When a particle placed inside an electromagnetic field, they accelerate due to a force which is called the Lorentz Force expressed as [3]:

$$d\frac{mv}{dt} = F = q[E + (v\ X\ B)] \qquad (\mathbf{1.1})$$

where "m" is the mass of the body, "v", the linear velocity of the body, "q", the charge carried by the body, "E", the electric filed and "B", the magnetic field. The size of the body is assumed to be negligible. The magnetic component of the electromagnetic field and the mass of the body is constant. So that the equation 1.1 becomes:

$$a = \frac{qE}{m} \qquad (\mathbf{1.2})$$

There is a force occurring so that the motion due to this force can be defined as Electrophoresis. The movement of charged particles in a fluid under an electric field

is Electrophoresis, and this movement only affects charge carrying bodies whether the field is uniform or nonuniform [13].

A dielectric particle placed in an electric field becomes electrically polarized as a result of partial charge separation. The charge separation leads to an induced dipole moment. In a non-uniform electric field, the particle experience Dielectrophoretic force and the force is defined by equation 1.3.

$$\overrightarrow{F_{D^E}}_P = 2\pi r^3 \varepsilon_0 \varepsilon_m \, Re[k(w)] \nabla E^2 \qquad (\mathbf{1.3})$$

Where r is a radius of the particle, w is the angular frequency of the applied field, ∇E denotes the electric field gradient and Re[k(ω)] is the real part of the Clausius-Mossoti factor.

According to the equation 1.3, the DEP force is controlled by the CM factor, which is frequency-dependent. CM factor (K(ω)) is expressed as

$$(\varepsilon^*_p - \varepsilon^*_m)/(\varepsilon^*_p + 2\varepsilon^*_m) \qquad \mathbf{(1.4)}$$

Where ε∗p is the complex permittivity of particles and ε∗p is the complex permittivity of the medium. The complex permittivity ε∗ is given by

$$\varepsilon - j\sigma/w \qquad \mathbf{(1.5)}$$

where $j=\sqrt{-1}$, σ is the material conductivity and ω is the angular frequency.

DEP depends on conductivity control at the low-frequency and the permittivity control at the high-frequency. There are two main cases that reveal the relationship between applied signal frequency and Re[$K(\omega)$]. The first case is when $\sigma_p < \sigma_m$ and $\varepsilon_p > \varepsilon_m$; making Re[$k(w)$] negative at low frequencies and positive at high frequencies and second case is when $\sigma_p > \sigma_m$ and $\varepsilon_p < \varepsilon_m$, where Re[$K(\omega)$] becomes positive at low frequencies and negative at high frequencies. Figure 1.10 illustrates the relationship between the applied signal frequency and Re[$K(\omega)$] with respect to the particle and the surrounding medium permittivity and conductivity [2].

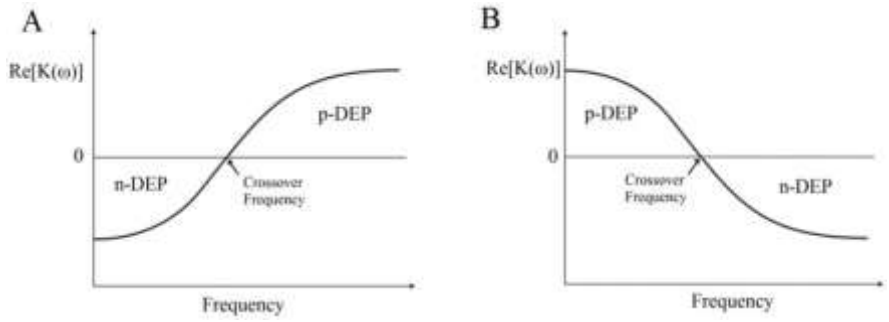

Figure 1.10 DEP spectrum (Re[K(ω)] vs. frequency) of a polarizable particle [2]

Despite the mentioned parameters, the operating voltage reduction can be achieved by reducing the size of electrodes that can attain similar DEP force on the particle as compared to the conventional method. Lower operating voltages also enables a reduction in electrical heating and electrochemical effects [15].

1.8 Giant Unilamellar Vesicles

A unilamellar vesicle is a circular shaped chamber/vesicle which consists of a single bilayer of an amphiphilic lipid. It is prepared by diluting the lipid in aqueous solution using a special setup. It is an artificially prepared model cell, equivalent to the cells in biological systems.

These type of vesicles fall under three groups according to their size:

- small unilamellar vesicles (SUVs)
- large unilamellar vesicles (LUVs)
- giant unilamellar vesicles (GUVs)

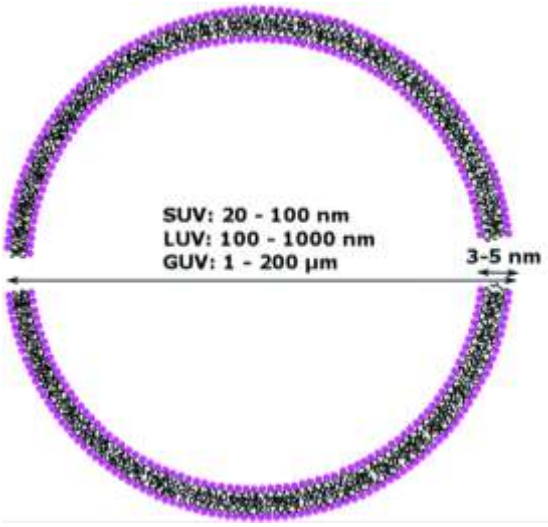

Figure 1.11 Schematic of unilamellar vesicles and their size distribution [32]

SUVs are usually prepared by sonication using a cup-horn, bath, or probe tip sonicator. LUVs can be prepared by a variety of methods including extrusion, detergent dialysis, a fusion of SUVs, reverse evaporation, and ethanol injection. Unilamellar vesicles are the large "onion-like" structures formed when amphiphilic lipids are hydrated. SUVs are typically 15-30nm in diameter while LUVs range from 100-200nm or larger. LUVs are stable on storage, however, SUVs will spontaneously fuse when they drop below the phase transition temperature of the lipid forming the vesicle. The Schematic of unilamellar vesicles and their size distribution is shown in Figure 1.11.

Angelova and Dimitrov discovered Electroformation of GUVs in 1986. As mentioned above, it is a way to prepare GUVs by modulating natural swelling of lipids hydrated with an aqueous buffer under the effect of alternating current with a certain frequency. Generally, Lipids are dissolved in chloroform and are placed on a conductive indium tin oxide coated glass, followed by evaporation of chloroform and dehydrating the dried lipids with buffer. The another ITO glass slide is then placed over the first ITO in the form of a sandwich. A sinusoidal alternating voltage is applied across the ITOs, initiating the GUV formation process. Figure 1.12 shows the Schematic of electroformation [29] and optical image of GUVs [35]. The significant pros of electroformation are

- No need for having expertise in the field to implement the process.

- High Yield
- Uniformity throughout the membrane.

However, the cost of the electrodes material is concerned, some are cheap but not providing high yield or tedious to clean after use and others are too expensive to afford.

But recently in 2017, researchers found new materials to perform electroporation likewise Valerio Pereno et al demonstrated the preparation of GUVs from DPhPC (1,2-dioleoyl-sn-glycero-3-phosphatidylcholine) on stainless steel electrodes (commercially available syringe needles) without facing any problem of lipid oxidation and/or hydrolysis [29].

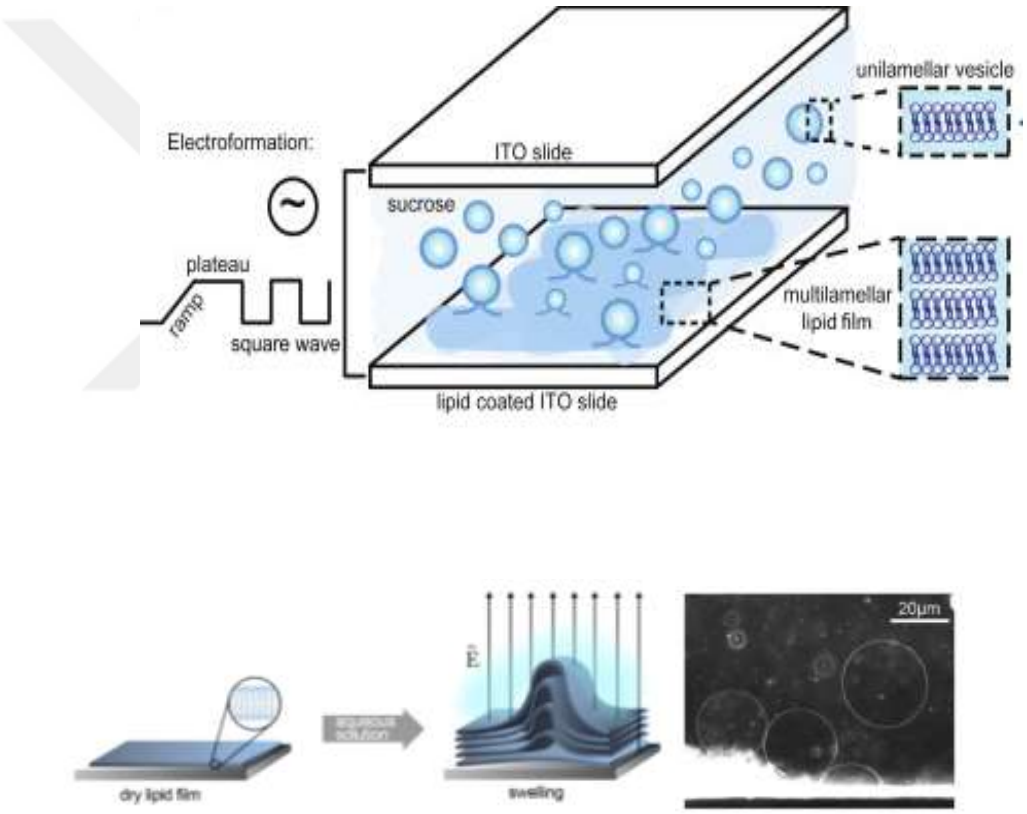

Figure 1.12 Schematic of electroformation [35] and optical image of GUVs [29]

Nowadays, Electroformation can be done with different materials. Table 1.5 compares the costs, advantages, and disadvantages of different materials during Electroformation.

Table 1.5 Comparison of Costs, Advantages, and Disadvantages of different materials during Electroformation [29]

	Cost	Disposable	Cleaning	Machinable	Scalable
Platinum	Expensive	No	Yes	Yes	Yes
ITO	Average	Yes	Yes	No	Yes
Stainless Steel	Cheap	Yes	Only If Reused	Yes	Yes

GUVs are used for different application such as

- Drug delivery: Drug carrying cosmetics like moisturizers to prevent from ultraviolet radiation.
- Biomedical research: To study biological systems because GUV's structure mimics the functions of real cells.

1.9 Antibiotic Permeability

1.9.1 Antibiotics

An antibiotic is a type of antimicrobial substance active against bacteria and is the most important type of antibacterial agent for fighting bacterial infections. For this study, norfloxacin which is from fluoroquinolones family, with broad-spectrum antibacterial activity against most gram-negative and gram-positive bacteria has been used. Norfloxacin inhibits bacterial DNA gyrase. The bactericidal action of Norfloxacin results from inhibition of the enzymes topoisomerase II (DNA gyrase) and topoisomerase IV, which are required for bacterial DNA replication, transcription, repair, and recombination. Norfloxacin is a broad-spectrum antibiotic agent that is shown to be effective against various Gram-positive and Gram-negative bacterial species. The fluorine atom at the 6 position increases potency against gram-negative organisms, and the piperazine moiety at the 7 positions is responsible for anti-pseudomonal activity. Figure 1.13 shows the Structure of Norfloxacin [1].

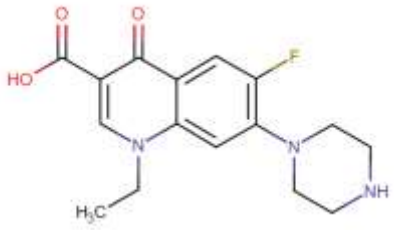

Figure 1.13 Structure of Norfloxacin [1]

1.9.2 Permeability

An antibiotic can permeate into the cell wall of bacteria in two ways.

- Active transport
- Passive transport

The bacteria wall is an obstacle to be crossed. Some of the bacterial walls are hydrophilic such as gram-negative bacteria, so most antibiotics can cross the outer membrane by passive diffusion without having pores in the walls and active diffusion through pores composed of 'porin' proteins. Uptake varies with the drug's charge, size, and hydrophilicity, also with the number of pores. Figure 1.14 displays the transportation of particles through the membrane is passive permeability and via membrane containing porins is active permeability [39].

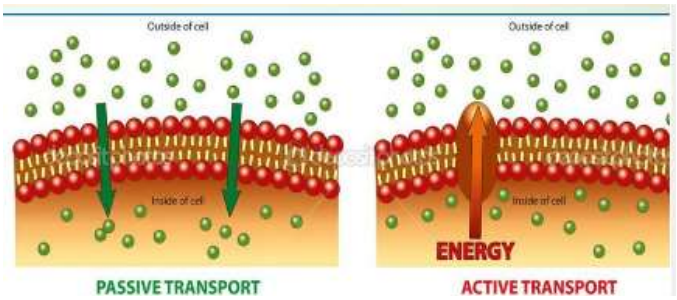

Figure 1.14 Transportation of particles through the membrane is passive permeability and via membrane containing porins is active permeability [39]

1.10 Summary

In this chapter, all terminologies related to the study are elaborated in detail. Moreover, the basic idea to approach for the accomplishment of this project is also given which can assist to understand the following chapters.

Chapter 2 introduces the required material and overall process used for the preparation of giant unilamellar vesicles in steps.

Chapter 3 explaines the fabrication of chip 1 and chip 2. The designing of chip using different softwares, materials used for fabrication and fabrication process such as standard lithography techniques are elaborated in detail.

Chapter 4 demonstrates the experimental aproach which is on chip and off chip experiments. The in house developed setup for electroformation is given and the method is revealed.

Chapter 5 sheds light on the results obtained from experiments. The gaussian distribution of GUVs is shown to show the count of vesicles prepared through electroformation using protocol. Also, off chip and on chip experiments explains the antibiotic permeability rate through the vesicles. The eletrochemical signal obtained from the an LCR meter represents the penetration of antibiotic thorough GUVs.

Chapter 6 concludes this project while explaining each chapter briefly. The future works is also envisioned as extention of this study.

CHAPTER 2

PREPARATION OF GIANT UNILAMELLAR VESICLES

2.1 Materials

To generate the Gaint Unilamellar Vesicles, Electroformation method has chosen among other methods due to the high yield of GUVs (10-100um). The required material is De-ionized water (to prepare all solutions followed by filtering with 0.45um filter (ISOLAB), Acetone, Isopropanol, Ethanol (for cleaning), DPhPC (1,2-diphytanoyl-sn-glycerol-3-phosphocholine) in powdered form (Avanti polar lipids), Chloroform, Sucrose (Aldrich Sigma), Octyl-polyoxyethylene (OPOE), TRIS (to increase the pH), Hydrochloric acid (to decrease the pH), Two Indium Tin Oxide Slides (Coverslip Thickness) Of 28 – 30 Ohm-Meter, Silicon Spacer (Few mm), Copper Strips Of Few Mm, Multimeter, Function Generator (GWINSTEK SFG-2107), BNC Connector, Digital Oscilloscope (RIGOL DS1052D), Optical Microscope (inverted (Euromex oxion Inverso)), Heater (ISOLAB), Pipettes, Pipette Tips, Tubes (For Collecting Samples), pH stripes or pH meter, Desiccator, Silicon Spacer, Vortex equipment, Weighing machine, Ultrasonic water bath. Figure 2.1 shows the required materials and set up for generating GUVs.

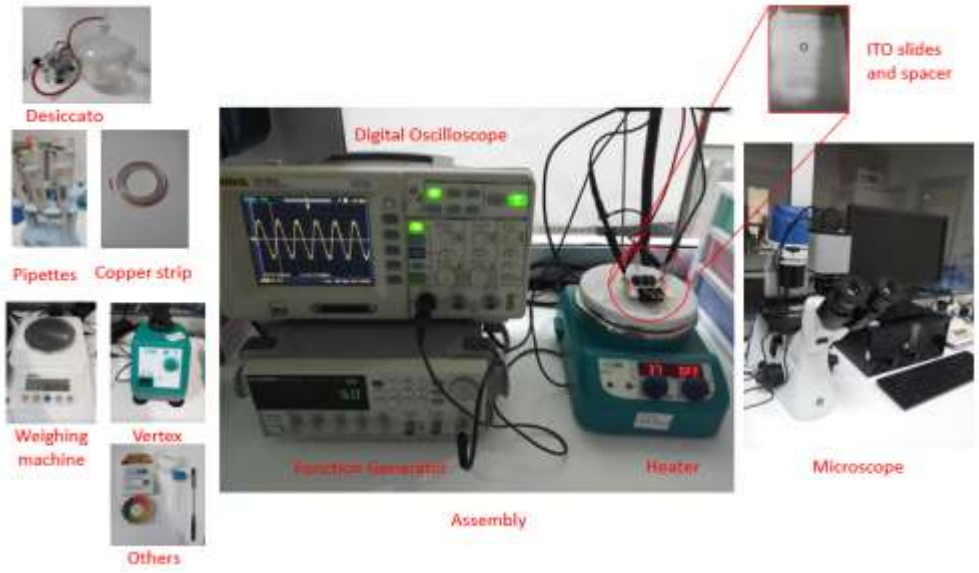

Figure 2.1 Required materials and set up for generating GUVs

2.2 Preparation of Aqueous solutions:

Sucrose: The molecular weight of sucrose is known as i.e 342.29 mol/liter. The concentration required is 200mM. we can easily find the sucrose in grams needed to prepare in 10 ml DI water by using formula (6).

$$M_1V_1 = M_2V_2 \qquad (\mathbf{2.1})$$

Tris: For preparing 1M of tris solution the same formula can be used.

Norfloxacin: The required concentration of NF is 2mM, so the same formula was used.

To change the pH of the NF solution to 5, 7, 9, the tris and hydrochloric acid were used.

2.3 Production of GUVs.

2.3.1 Preparation of phospholipid stock solution

Weigh 5mg phospholipid (1,2-diphytanoyl-sn-glycero-3-phosphocholine (DPhPC)) (Avanti Polar Lipids) and dissolve the powder in 1 ml chloroform.

2.3.2 Electroformation

Initially, the ITO glass slides should be cleaned with DI and Ethanol (70:30) properly. If possible the plasma cleaning is recommended to clean the surface of ITOs.

Step 1: Identify the conductive sides of the ITO-slides with a multimeter.

Step 2: Use a 100µl Hamilton syringe to spread 60µl of phospholipid stock solution on one of the ITO glass slides.

Step 3: Leave the ITO coating side upwards into a vacuum desiccator for 10 min.

Step 4: Prepare 200 mM sucrose solution, dissolve it in 1M Tris Buffer to achieve pH 7, vortex until sucrose is dissolved.

Step 5: Use tweezers to place the ITO-slide lipid film point upwards. Place silicon spacer around the dried lipid film, add 600µl of 200 mM sucrose solution into the spacer.

Step 6: Place a second ITO-slide on top of the spacer with the conductive side facing downwards using tweezers.

Step 7: Use a paper binder to hold the assembly together and carefully, place the ITO assembly on the heater at 37.5˚C.

Step 8: Connect the assembly with a function generator and digital oscilloscope according to Table 2.1 and Figure 2.2.

Table 2.1 The parameter of Electroformation method

Time	Frequency	Voltage	Temperature
5 minutes	5 Hz	0 to 3 Vpp	37.5˚C
2 hours	5 Hz	3 Vpp	37.5˚C
5 minutes	5 Hz	3 to 0 Vpp	37.5˚C

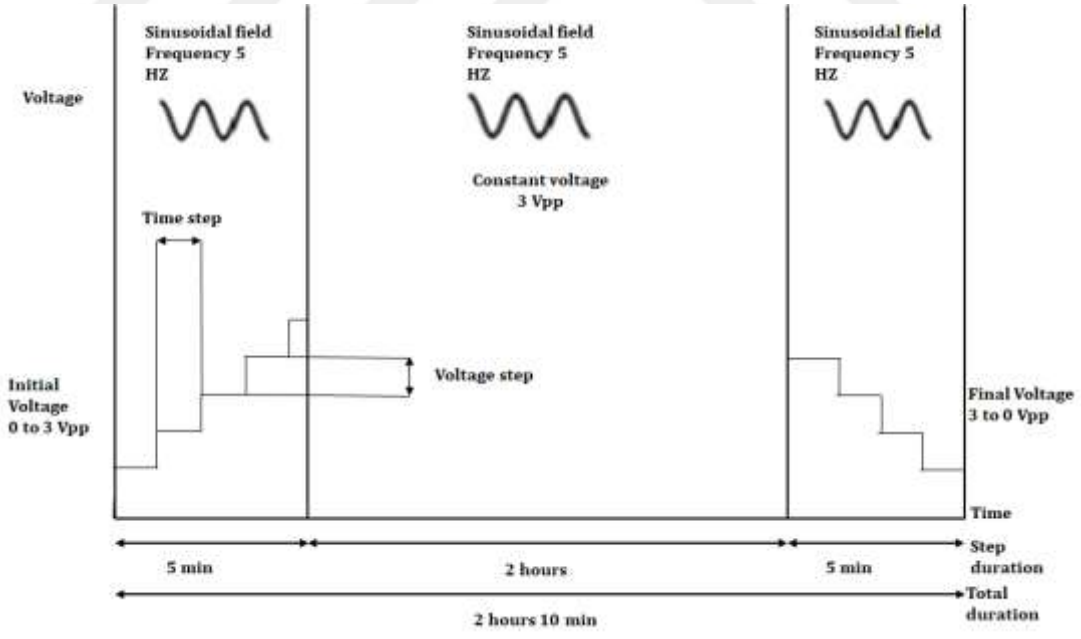

Figure 2.2 Protocol for Electroformation technique [5]

Step 9: After the protocol ends to remove the assembly from the heater. Remove the paper binder and use the tweezers to remove the top ITO-slide.

Step 10: Take a pipette and tip to collect the sample from the ITO-slide surface slowly.

Note: Lipid stock solutions should be placed at -80-degree C!

2.3.3 OmpF Incubation to Vesicles

Step 11: Take 5.5 mg purified stock of OmpF and detergent (1% solution of OPOE) in 1 ml of deionized water (Jehangir Cama et al., 2015b).

Step 12: Add 2.5 ul diluted OmpF solution to 500 ul GUVs.

Step 13: Keep it aside at room temperature for incubation.

Step 14: Add bio beads to the incubated solution, to remove the detergent, followed by storing overnight in the refrigerator.

Step 15: Next day, take a pipette and tip to collect the OmpF infused proteo-GUVs carefully.

Step 16: Pour the tiny droplet of prepared GUVs on a cleaned glass slide and observe the GUVs and pro-GUVs under a microscope and save the images to analyze the size distribution.

Note: The OmpF protein was produced by Dr. Cihan Darcan and Ozge Kaygusuz at Bilecik Şeyh Edebali University.

2.4 Summary

The in-house developed electrofornation setup has been installed successfully. The material required for the process is explained. The aquesous solutions were prepared in deionized water. protocol used for electroformation is described in steps. The porins were successfully attached to the GUVs obtained.

CHAPTER 3

CHIP FABRICATION

In this study, two chips have been produced for experimentation. Chip 1 was fabricated at Istanbul Technical University (ITU) and chip 2 was prepared at Ankara Yildirim Beyazit University. In ITU, experiments were carried out at Nano-Micro Engineered and Manufacturing System Laboratory in Istanbul Technical University, together with Hatice Turhan,Alp Gürkaynak and Mehmet Tugrul Birtek under the co-supervision of Prof. Dr. Levent Trabzon. The following sections explain the fabrication procedure for each chip.

3.1 Fabrication of Chip 1

The fabrication process of the designed microfluidic chip 1 is the same as written in B.Sc. thesis of the student from ITU, MEMS laboratory [28].

3.1.1 Production of Electrode Array

Electrode array production involves the pattern mask lithography, mask development, etching, substrate preparation, spin coating, substrate photolithography, photoresist developing, physical vapor deposition and lift-off steps.

3.1.1.1 Pattern Mask Lithography

PCB design software Klayout v0.23.10 (Matthias Köfferlein) and L-edit v13 (Tanner EDA, California, U.S.A) was utilized to draw the design for the electrode array. The .GDSII format of drawing was converted into .JOB format using conversion software (Heidelberg Instruments Mikrotechnik GmbH). The pattern masks were written on 120mm×120mm×8mm dimensional chromium plate after coated with a 540nm thick positive photoresist (AZ1500, CS Hardmask Blanks, Clean Surface Technology Co., Kangawa, Japan) using a 4mm write head on a DWL 66FS series High-Resolution Pattern Generator (Heidelberg Instruments Mikrotechnik GmbH., Heidelberg, Germany).

3.1.1.2 Mask Development and Etching

After exposure, the positive photoresist was baked and developed in an AZ 351B solution (Microchemicals GmbH, Ulm, Germany) for 40 seconds. The development of the photoresist was first assessed qualitatively for color changes indicating underdevelopment under an Axio Imager Upright Microscope (Carl Zeiss Jena GmbH, Thüringen, Germany) then the features were measured to assess the accuracy of the pattern. The exposed chromium coating was removed using Etch-18 Chromium etchant (Microchemicals GmbH, Ulm, Germany). After this step, the etching procedure was qualitatively assessed under the same optical microscope (Figure 3.1). The remaining photoresist was removed with acetone and the pattern mask was cleaned with isopropyl alcohol, rinsed with water followed by blow drying with nitrogen gas.

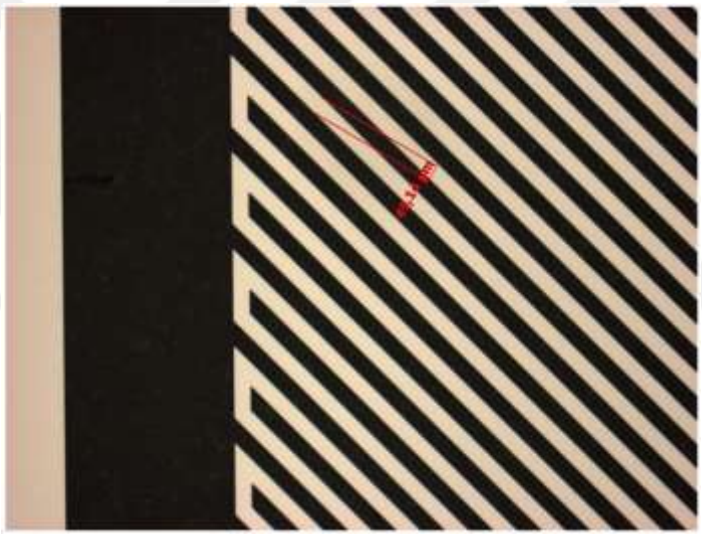

Figure 3.1 Electrode spacing accuracy

3.1.1.3 Substrate Preparation

35mm×25mm×3mm substrates were prepared by cutting 70mm×25mm×3mm microscope slides (Gold Seal Products, Hungary) cleaned with 1M KOH solution for 10 minutes and with acetone for 10 minutes at 35kHz using a UW Qi-100 ultrasonic cleaner (Ultrawave Precision Ultrasonic Cleaning Equipment, Cardiff, U.K.). The substrates were then rinsed with isopropyl alcohol and followed by DI-water and blow-dried with nitrogen gas.

3.1.1.4 Spin Coating

After cleaning, the substrates were coated with a 400 nm thick positive photoresist (AZ1500, Microchemicals GmbH, Ulm, Germany) on WS-400-6NPPB single substrate spin processor (Laurell Technologies Corporation, North Wales, U.S.A) finishing by soft baking at 100°C for 50 seconds.

3.1.1.5 Photolithography and Development

The photoresist coated substrates were then placed on a Suss MA6 mask aligner (SUSS MicroTec, Garching, Germany) along with the pattern mask prepared earlier and exposed to 850W, 365 nm UV light source using contact printing.

After exposure, the photoresist on the substrates was developed in positive developer (AZ 351B, Microchemicals GmbH, Ulm, Germany) for 15 seconds and rinsed with DI water. The development was assessed in the same manner as it was done for the pattern mask and the photoresist was hard baked for the 50s at 115°C. All processes involving photosensitive chemicals were carried out in a 100 class laminar flow cleanroom installed with 589 nm emitting lights.

3.1.1.6 Physical Vapour Deposition and Lift-off

The glass substrates prepared earlier were placed in a custom built thin film deposition chamber (Kurt J. Lesker Company, Pennsylvania, U.S.A.), the pressure was decreased to 7.8×10^{-7} torr and the substrates were axially rotated at 12 rpm. A 200nm layer of 99.995% purity Titanium supplied by Kurt J. Lesker Company was deposited on the substrates at a rate of 7 nm/min. The deposition was done by the Electron Beam PVD technique using 10KV and 60mA. After deposition, the substrates were kept in vacuum for an hour before starting the lift-off process.

The lift-off process was done by submerging the specimens in acetone and cleaning them in a UW Qi-100 ultrasonic cleaner (Ultrawave Precision Ultrasonic Cleaning Equipment, Cardiff, U.K.) at 35 kHz for 15 minutes. The specimens were then rinsed first with isopropyl alcohol then with DI water and blow dried using nitrogen gas.

3.1.2 Production of Microfluidic chip

Microchannel fabrication involves the same steps as above mentioned for electrode array production except PDMS casting. The channel pattern mask was developed in the same manner as the electrode pattern mask, indeed both designs were prepared together and etched on the same substrate. A negative Photoresist coating was used for spin coating a 100mm silicon wafer. Then the after lithography, the obtained template was used as a mould for microchannel.

3.1.2.1 Microchannel Casting

Sylgard ® 184 Polydimethylsiloxane (PDMS) silicone elastomer and curing agent (Dow Corning, Minnesota, U.S.A.) were taken in 10:1 ratio and thoroughly mixed and poured in the petri dish containing template fabricated earlier. Then the vacuum chamber was turned on at 50 mBar and the mixture was placed to remove bubbles to avoid defects. Then for 15 minutes, the template transferred on to the heater set at 115°C.

When it was done the poking test at the edge of cured PDMS layer assured to peel off PDMS around the microchannel by cutting it carefully followed by punching 0.5mm holes for the syringe attachment.

3.1.3 Assembly

The faces of the PDMS microchannel and the glass slide with the electrode array placed upside on glass sheet inside a PDC-32G-2 plasma cleaner (Harrick Plasma, New York, U.S.A.). The surface of the glass substrate was wetted with methanol and the microchannel was placed on top of the methanol layer to prevent the parts sticking prematurely before proper alignment was made, immediately after removing from the plasma cleaner.

The parts were aligned manually under an Olympus BX51 System Microscope (Olympus Corporation, Tokyo, Japan) using the alignment features etched on to the pattern mask. The aligned chip was placed in a vacuum chamber and kept in 55°C temperature and under 50 millibar pressure for 15 minutes to remove all the methanol. After this step, the alignment of the now fused parts was checked one again under the same optical microscope. Copper electrical wires were attached to the electrode

terminals on the chip using Cold Solder Silver Epoxy electrically conducting adhesive (M.G. Chemicals, Ontario, Canada) and the chip was kept on a hotplate set to 65°C for 15 minutes to cure the epoxy. The finished chip is shown in Figure 3.2.



Figure 3.2 Finished view of lab-on-chip

3.2 Fabrication of Chip 2

The fabrication process of the designed microfluidic chip is divided into three stages:

1. Designing of the integrated microfluidic chip
2. Fabrication of the electrode array
3. Production of the microfluidic channels
4. Integration of the produced parts

All processes were carried out in a cleanroom at AYBU.

3.2.1 Designing of Microfluidic Chips

Microfluidic chip design which consists of microchannels and 6 electrodes separated with a gap of 50um from the center to be placed underneath as shown in Figure 3.3. Length of the channel from T junction = 386 mm

- Horizontal channel width = 200 um
- Vertical channel width = 300 um
- Electrode width = 100 um
- Gap between electrode fingers = 50 um

- Total length of per electrode = 10.975 mm

The channel design has two inlets for receiving a solution containing GUVs and Norfloxacin and an outlet for collection of NF loaded GUVs. Figure 3.3 2D and 3D view of the main parts of a microfluidic chip

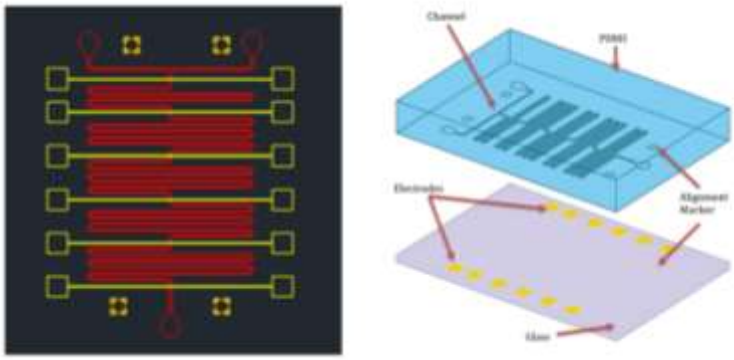

Figure 3.3 2D and 3D view of the main parts of a microfluidic chip

Computer Simulations are performed in COMSOL Multiphysics v5.4 to determine flow profile of microchannel is sketched in Figure 3.3.

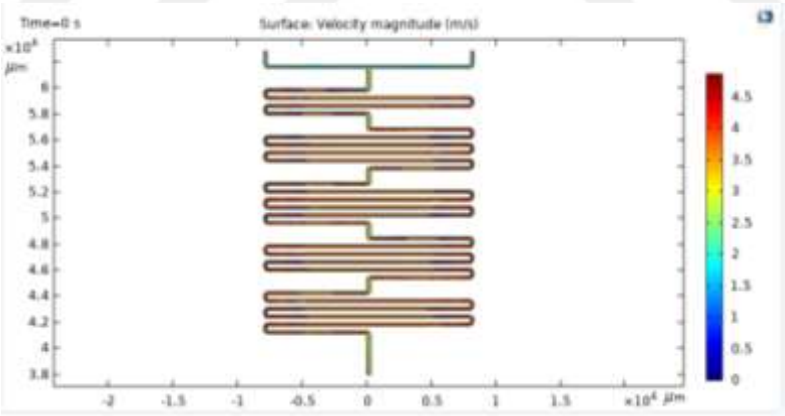

Figure 3.4 Velocity profile of the microfluidic channel

3.2.2 Production of Electrode Array

Electrode array production involves the following steps:

1. Mask development
2. Substrate preparation

3. Spin coating (figure 3.5 – 1)
4. Substrate photolithography (figure 3.5 – 2)
5. Sputtering (figure 3.5 – 3)
6. Lift-off process (figure 3.5 – 4)

Figure 3.5 displays the process flow of fabrication.

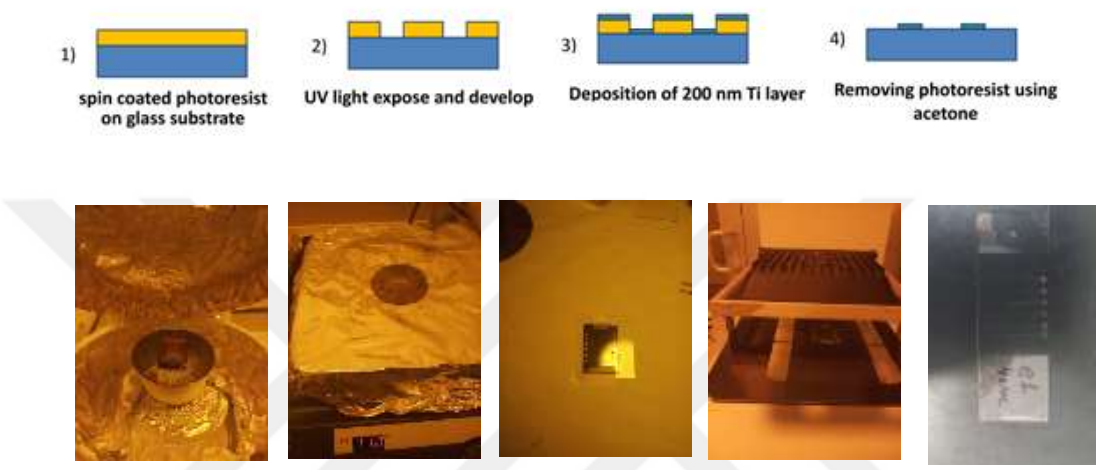

Figure 3.5 Flow diagram of fabrication (schematic and practical)

3.2.2.1 Mask production

The masks were designed on AUTOCAD and then transfer to CORELDRAW for high resolution. The pattern masks were saved as .pdf format and printed on acetate paper from COZUM TANITUM. Photomask can be seen in Figure 3.6.

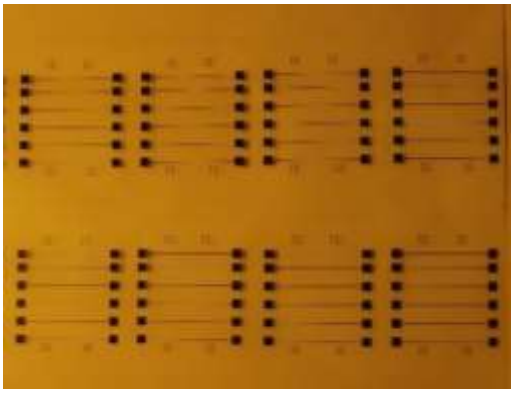

Figure 3.6 Photo Mask of the electrode

3.2.2.2 Substrate preparation

Microscope slides were cut in half and the prepared substrates were cleaned first in 1M KOH solution for 10 minutes then in acetone for 10 minutes using an ultrasonic cleaner. The substrates were then rinsed with isopropyl alcohol and then with water and blow-dried with nitrogen gas.

3.2.2.3 Spin Coating

After cleaning, the substrates were stuck on a silicon wafer for fine placement on the chuck of a spin coater. Then the substrates were coated with 2.5 ul positive photoresist AZ-9620 using single substrate spin processor. Before exposure, the photoresist coating was soft baked for 2 minutes 45 seconds at 110°C. gas. Spin coating and soft baking can be seen in Figure 3.7.

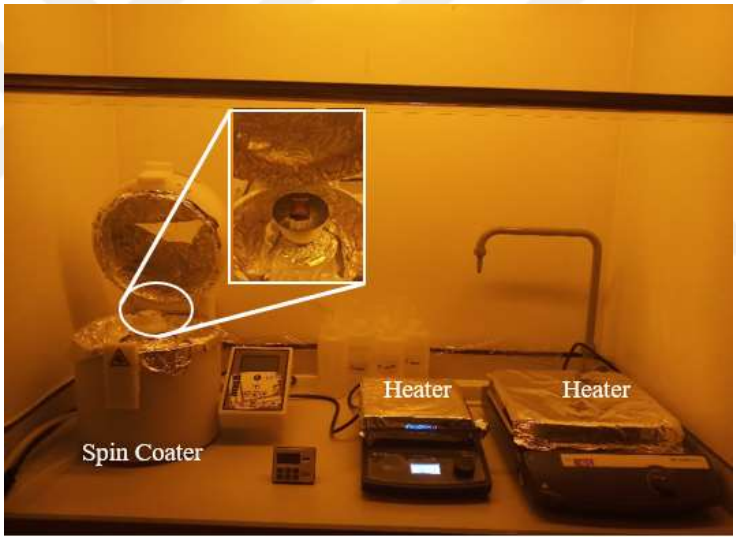

Figure 3.7 Setup of spin coating and baking

3.2.2.4 Photolithography

The photoresist coated substrates were placed on the pattern mask prepared earlier with scotch tape (Figure 3.8) and exposed to in-house developed UV light source (Figure 3.9) for 70 seconds in contact configuration.

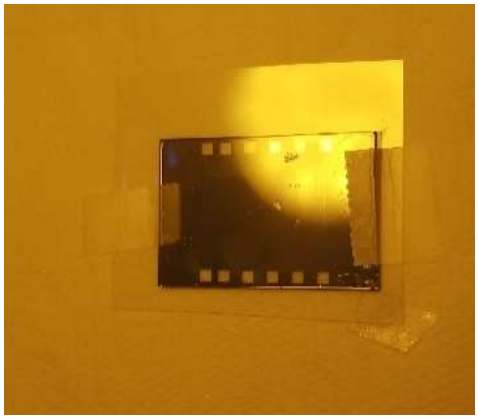

Figure 3.8 The photomask of the electrode is placed on PR coated glass slide

After exposure, the photoresist on the substrates was developed in a positive developer (TEAH) for 2 minutes 30 seconds and rinsed with DI water. These parameters are optimized by undertaking multiple trials conducted by Iremnur. There is no need for hardbake before sputtering according to the datasheet.



Figure 3.9 The pasted photomask of the electrode over PR coated glass slide rested under the in-house developed UV light source

3.2.2.5 Sputtering

The glass substrates prepared earlier were placed in a sputtering chamber at ITU. A 200nm thick layer of Titanium was deposited on the substrates at a rate of 7 nm/min.

This deposition technique is one of the PVD techniques. After deposition, the substrates were kept in vacuum for an hour before proceeding to the lift-off process. The sputtering can be seen in Figure 3.10.



Figure 3.10 sputtering process

3.2.2.6 Lift-off

The lift-off process was done by submerging the specimens in acetone and cleaning them in an ultrasonic cleaner for 15 minutes. The specimens were then rinsed first with isopropyl alcohol than with DI water and blow dried using nitrogen gas. After development, the accuracy of the features was assessed under a microscope.

3.2.3 Production of Microfluidic Channels

Microfluidic channel fabrication involves:

1. Mask Development
2. Spin coating
3. Photolithography
4. PDMS casting

Figure 3.11 displays the process flow of fabrication.

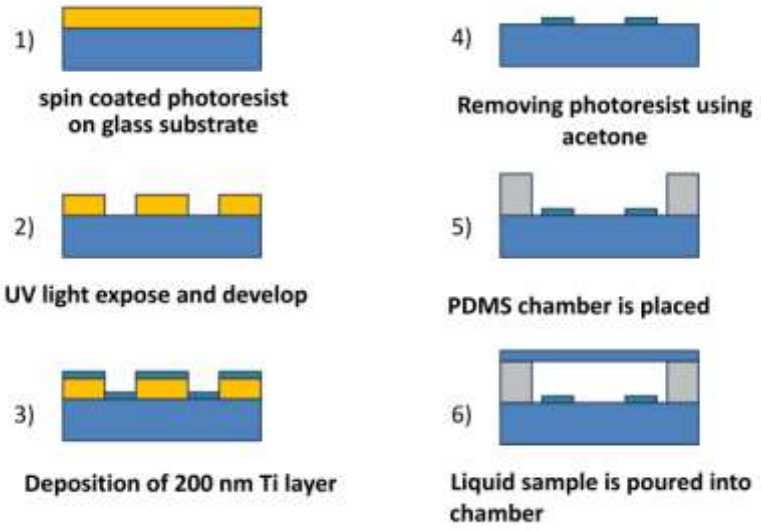

Figure 3.11 Flow diagram of fabrication

3.2.3.1 Mask production

The channel pattern mask was developed in the same manner as the electrode pattern mask (Figure 3.12), indeed both designs were prepared together and printed on the same acetate paper.

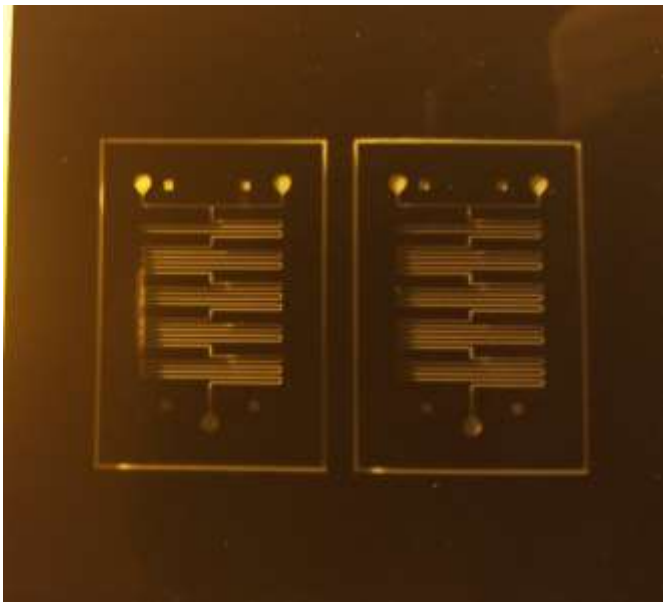

Figure 3.12 Photomask of the microfluidic channel

3.2.3.2 Spin Coating

A silicon wafer was cleaned first with acetone then with isopropyl alcohol and lastly rinsed with DI water. The wafer was then blow dried using nitrogen gas and left on a hot plate set to 115 °C for 15 minutes. The silicon wafer was placed on a chuck and 3 ml negative photoresist SU-8 2050 was coated by spinning at program 4. After spin coating, the photoresist was sot baked for 3 minutes at 65°C and 6 minutes at 95 °C. Spin coating and soft baking can be seen in Figure 3.13.

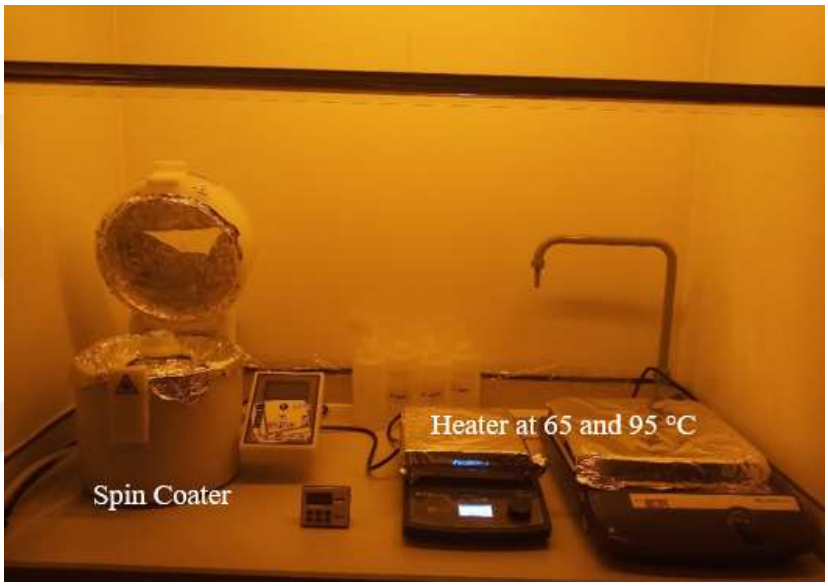

Figure 3.13 Setup of spin coating and baking

3.2.3.3 Photolithography

The photoresist coated wafer and the pattern mask were pasted together and exposed to an in-house developed UV light source for 200 seconds in contact configuration. Immediately after exposure to UV light, the wafer was placed on a hotplate set to 65°C for a minute and 95°C for 6 minutes for a post-exposure bake. Once the post-exposure bake was complete the wafer was submerged in a puddle of developer solution (PMA) in a petri dish and the petri dish was gently shaken for 3 to 5 minutes for the development of the photoresist. The wafer was then removed from the puddle, rinsed with isopropyl alcohol and DI water and blow-dried with nitrogen gas. The developed template can be seen in Figure 3.14.

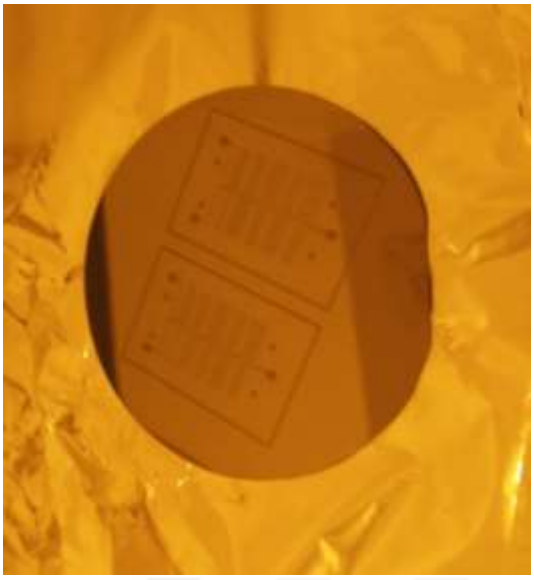

Figure 3.14 Fabricated template on a silicon wafer

Note: the whole fabrication process should be taken place in clean room installed with yellow light. Because photoresist is very sensitive element and it reacts in normal light so a particular wavelength of light can avoid distortion in the process.

3.2.3.4 PDMS Casting

Poly-dimethyl siloxane (PDMS) silicone elastomer and curing agent were thoroughly mixed for 2 minutes in 9:1 ratio. The template wafer with microchannel pattern was placed in a petri dish and PDMS mixture was poured on it. The petri dish was then placed inside a desiccator for 20 minutes to get rid of all the air bubbles caused by the mixing. Lastly, the petri dish was kept on a heater plate set to 60°C for more than 2 hours for hardening the PDMS. The weighing of the mixture, Pouring mixture on the wafer mold, keeping in a desiccator, curing the mixture over heater and bounding of cured PDMS over glass slide after peeling off from mold and cut from edges can be seen in Figure 3.15. When the curing process was complete by assuring with poking the edge of the PDMS layer with the end of a pair of forceps, the PDMS layer on top of the wafer was peeled off and the excess PDMS around the microchannel was cut out with a scalpel and 0.5mm holes were punched with a punching tool. Steps of the cutting out the area of microchannel can be seen in Figure 3.16.

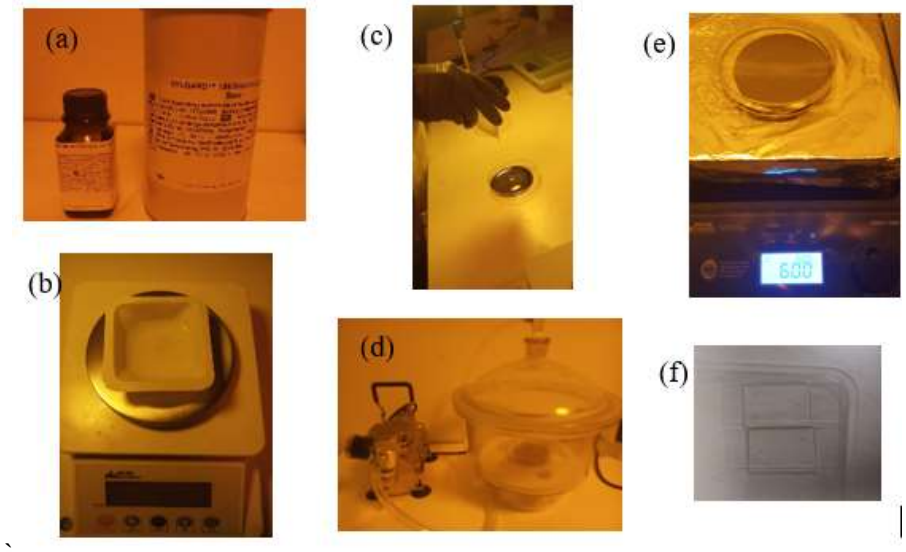

Figure 3.15 Steps to be followed to get the microfluidic chips

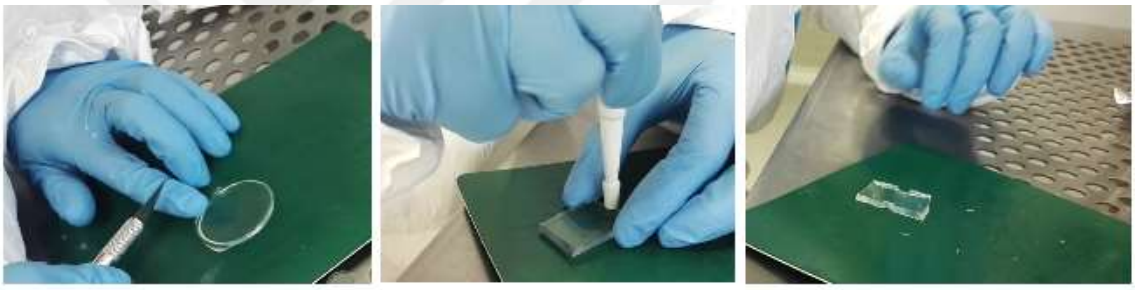

Figure 3.16 Cutting out the area containing microchannel

3.2.4 Integration of Microfluidic chip onto Electrode chip

The PDMS microchannel and the glass substrate with the electrode array were placed inside an in-house developed plasma cleaner with their surfaces to be stuck facing up and exposed to the plasma. The chamber was vacuumed and exposed by changing amperes from a power source. The manual alignment was made and can be seen in Figure 3.17.

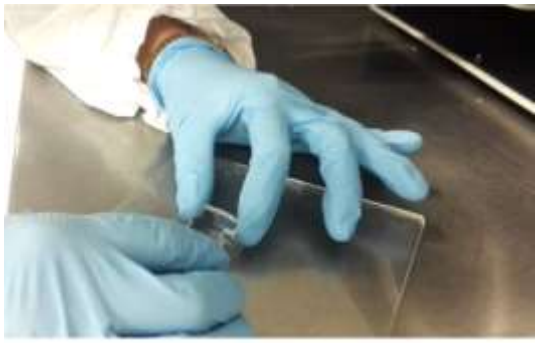

Figure 3.17 Manual alignment

The parts were aligned manually under a microscope using the alignment markers inscribed on to the pattern mask. The aligned chip was placed on the heater at 110°C for 2 hours. After this step, the alignment of the now fused parts was checked one again under the optical microscope.

Figure 3.18 shows that copper electrical wires attached to the electrode terminals on the chip using silver epoxy (electrically conducting adhesive) and the chip was kept on a hotplate set to 125°C for an hour to harden the epoxy.



Figure 3.18 Epoxy Bonding

3.3 Summary

Overall, chip 1 and chip 2 were designed and fabricated succesfully at ITU and AYBU respectively and evemtually, chip 1 was used for off-chip experiments and chip 2 was used for on-chip experiments.

CHAPTER 4

EXPERIMENTAL APPROACH

In this work, we aim to investigate the passive permeability (GUVs without porins-permeability through lipid bilayer) and active permeability (GUVs with porins-permeability through porins). The data obtained which is the variation in impedance and admittance can tell us the significant changes occur outside the GUVs.

Table 4. 1 Experimentation Methods

Ways to perform Experiments
Off-chip Testing 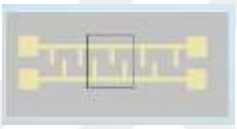
On-chip Testing 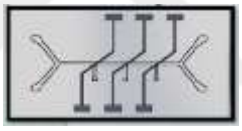

Table 4.2 Ways of antibiotic transport to GUVs

	Passive Permeability	Active Permeability
1.	GUVs	Porin-mediated GUVs
2.	GUVs + Antibiotics	Porin-mediated GUVs + Antibiotics

We have performed the conductivity measurements of the suspended solution with conductivity meter that can also assist to determine the changes in the medium. We performed the experiments in two sets: off-chip testing and on-chip testing for checking passive and active permeability, respectively (Table 4. 1 and Table 4.2).

4.1 Off-chip Experiments

The off-chip testing was carried out to check conductivity values with a conductivity meter and impedance measurement with LCR meter (HAMEG Instruments). The setup for both types of equipments is shown in Figure 4.1. The connections are made to the chip by alligator cords of the LCR meter. All experiments were repeated for 4 times at 1.5 V and 100 KHz.

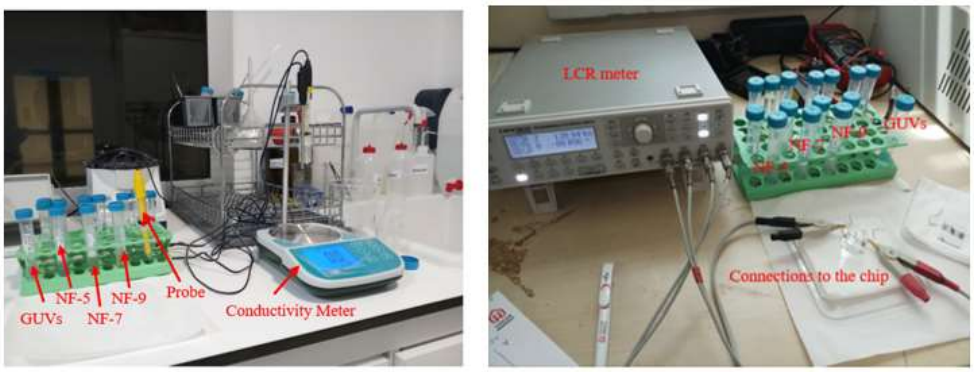

Figure 4.1 Conductivity Test Setup and Test equipment of impedance measurement

4.1.1 Conductivity Measurements:

500ul of GUVs was dissolved in 2.5ml of sucrose (200mM, pH:7) and 500ul of NF (pH:5, 7, 9) in three different tubes. The total volume for each tube is 3 mL.

4.1.2 Impedance Measurements:

The electrode array of chip 1 was used for the impedance and admittance measurements of NF loaded GUVs over time with an LCR meter. A very small sample of GUVs and NF(pH-5, 7, 9) was used i.e. 50 ul of GUVs and 10 ul of NF (pH-5, 7, 9).

4.2 On-chip Experiments

The on-chip testing was carried out to check impedance measurement with LCR meter. The integrated microfluidic chip produced was placed under an optical microscope and the electrodes were connected to an LCR meter. All of the wires and the chip itself were fixed on to the focal plane of the microscope with a sellotape or double-sided

tape. 0.5 mm plastic tubings were attached to the chip inlets. Figure 4.2 shows the entire setup for experimentation. All experiments were repeated for 4 times at 1.5 V and 100 KHz.



Figure 4.2 Entire set up

The time for the completion of the flow of GUVs and NF from inlets to the outlet was calculated by assuming the flow rate as 0.5 ul/min and 1 ul/min as shown in Table 4.3. and it was calculated by using the formula mentioned below:

- Velocity = displacement * time
- Flow rate = volume / time

  = (area * displacement) / time

  = area * velocity

Table 4.3 Time calculation for given flow rate

Flow rate	Time
0.5 ul/min	7.72 min
1 ul/min	3.86 min

- Conversion into m3/min
- So 0.5 ul/min = 5*10-10 m3/min and 1 ul / min = 1*10-10 m3/min

- Displacement = length of channel = 386 mm = 386*10-3 m
- Area = width * height = 200 um * 50 um = 0.01 m

4.2.1 Impedance Measurements:

The chip 2 has been used for the impedance and admittance measurement of NF loaded GUVs over time with an LCR meter. GUVs and NF (pH-5, 7, 9) were pumped through the channels at 0.5 ul/min flow rate with a syringe pump. The experiments were performed for 4 times and the results are discussed in further section.

4.3 Summary

An LCR meter and conductivity-pH meter were used for off-chip and on-chip experiments. The electrical connections were made with the aligator clips to the silver epoxy bonded copper wire to the chip. The readings were taken manually from the display of LCR meter and conductivity-pH meter.

CHAPTER 5

RESULTS AND DISCUSSION

In this section, firstly, the size distribution of the GUVs are discussed. Secondly, off-chip and on-chip experiments for the conductivity, impedance, and admittance measurements are represented.

5.1 Giant Unilamellar Vesicle

The electroformation experiments were performed for more than 10 times but best of 4 trials have chosen to present the size distribution. An optical image was taken by microscope (EUROMEX) at magnification 40X as shown in Figure 5.1.



Figure 5.1 The image of GUVs generated by Electroformation was taken by an optical microscope at magnification 40X. Scale bar is 10um

5.1.1 Gaussian Distribution

The size distribution analysis was performed using ImageJ software. The Gaussian curves were obtained via Origin Pro software to determine the size distribution curves and number of the GUVs. The trials were conducted for 4 times by varying the desiccator time to see if there is any change in the count of GUVs. Marie et al have

conducted the research to create GUVs from different lipids (DOPC, DLPC, and DHAPC) at different applied voltages for longer period of time [6]. They have concluded that the number of vesicles produced increased as the duration of the Electroformation increases or when the maximum applied voltage increases. However, in our experiments, we varied the rate of evaporation of chloroform from lipids and observed decrease in the size of vesicles after electroformation.

Moreover, we used DPhPC which has ideal bilayer-forming properties with wide temperature range (-120 to 120 C) and stability to oxidation. Other lipids can be used but some critical parameters should be avoided such as preparation conditions of GUVs, homogeneity or heterogeneity of membrane and so on. Whereas, the power supply parameters were kept constant such as voltage applied, duration of Electroformation, frequency, and temperature except for the evaporation time in a desiccator. The results obtained are shown as follows:

Figure 5.2 represents the size distribution of the produced GUVs at 5 min in a desiccator. The Gaussian fit of 4 trials is shown in Figure 5.2 depicts the overall mean of Gaussian curves. Table 5.1 explains the percentage of GUVs under 30 μm and above 30 μm. As it is clear from the table that the population of GUVs less than 30 um is around 92%.

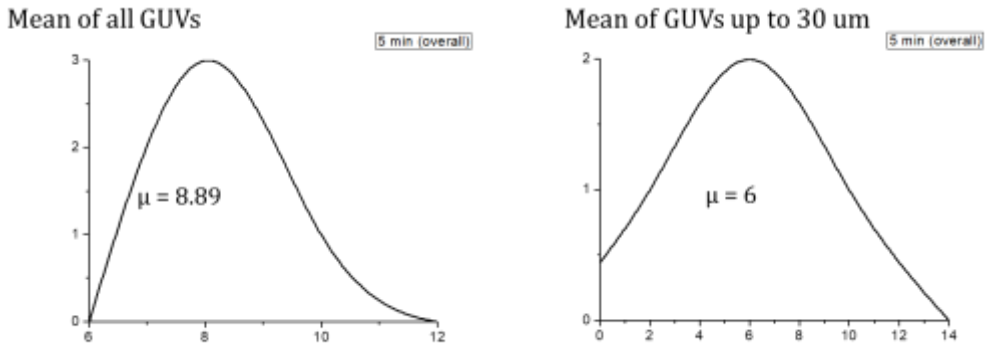

Figure 5.2 Comparison between the mean value of all size of GUVs and GUVs under the 30-um generated after keeping for 5 minutes in a desiccator

Table 5.1 The table shows the percentage of GUVs under and above 30-um generated after keeping for 5 minutes in a desiccator

Trials	<30	>30
5 min 1	88.6%	11.4%
5 min 2	91.42%	8.57%
5 min 3	95.71%	4.28%
5 min 4	92.85%	7.14%
Average	92.14%	7.85%

Figure 5.2 represents the size distribution of the produced GUVs at 10 min in a desiccator. The Gaussian fit of 4 trials is shown in Figure 5.2 depicts the overall mean of Gaussian curves. Table 5.2 explains the percentage of GUVs under 30 µm and above 30 µm. As it is clear from the table that the population of GUVs less than 30 um is around 95%.

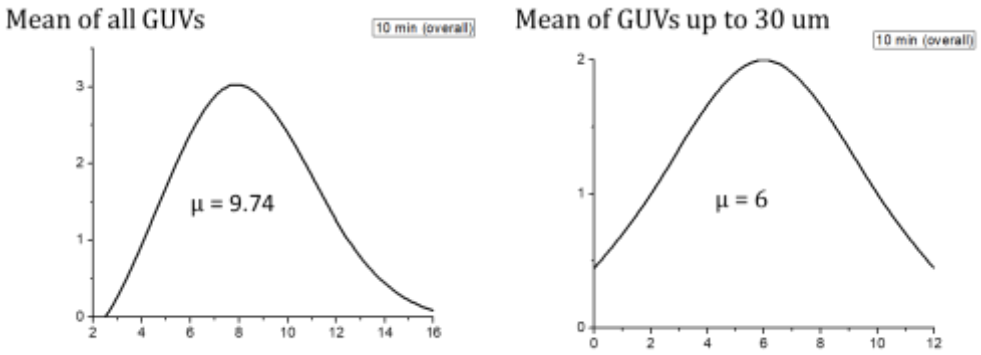

Figure 5.3 Comparison between the mean value of all size of GUVs and GUVs under the 30-um generated after keeping for 10 minutes in a desiccator

Table 5.2 The table shows the percentage of GUVs under and above 30-um generated after keeping for 10 minutes in a desiccator

Trials	<30	>30
10 min 1	97.14%	2.85%
10 min 2	94.28%	5.71%
10 min 3	95.70%	4.28%
10 min 4	91.42%	8.57%
Average	94.64%	5.35%

Figure 5.4 represents the size distribution of the produced GUVs at 15 min in a desiccator. The Gaussian fit of 4 trials is shown in Figure 5.4 depicts the overall mean of Gaussian curves. Table 5.3 explains the percentage of GUVs under 30 µm and above 30 µm. As it is clear from the table that the population of GUVs less than 30 um is around 83%.

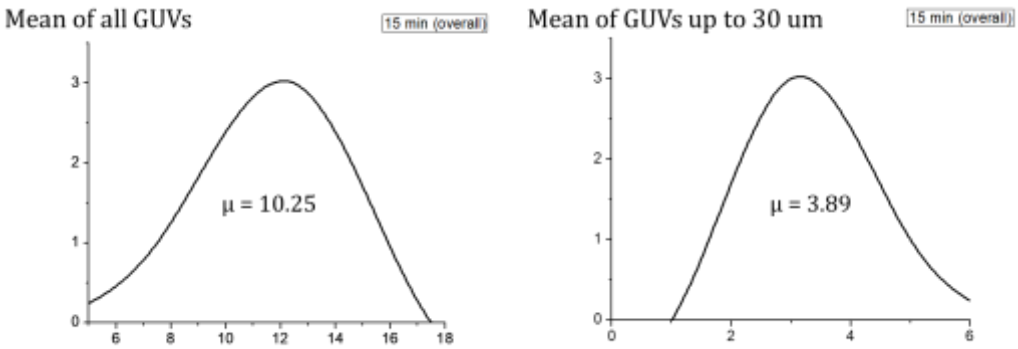

Figure 5.4 Comparison between the mean value of all size of GUVs and GUVs under the 30-um generated after keeping for 15 minutes in a desiccator

Table 5.3 The table shows the percentage of GUVs under and above 30-um generated after keeping for 15 minutes in a desiccator

Trials	<30	>30
15 Min 1	80.00%	20.00%
15 Min 2	85.71%	14.28%
15 Min 3	91.42%	8.57%
15 Min 4	72.85%	27.14%
Average	82.50%	17.50%

Figure 5.5 represents the size distribution of the produced GUVs at 20 min in a desiccator. The Gaussian fit of 4 trials is shown in Figure 5.5 depicts the overall mean of Gaussian curves. Table 5.4 explains the percentage of GUVs under 30 µm and above 30 µm. As it is clear from the table that the population of GUVs less than 30 um is around 86%.

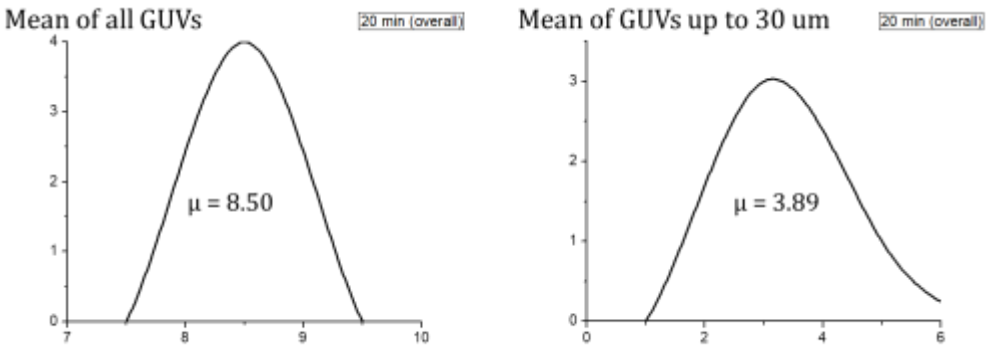

Figure 5.5 Comparison between the mean value of all size of GUVs and GUVs under the 30-um generated after keeping for 20 minutes in a desiccator

Table 5.4 The table shows the percentage of GUVs under and above 30-um generated after keeping for 20 minutes in a desiccator

Trials	<30	>30
20 min 1	92.85%	7.14%
20 min 2	92.85%	7.14%
20 min 3	77.14%	22.85%
20 min 4	82.85%	17.14%
Average	86.42%	13.57%

Figure 5.6 represents the size distribution of the produced GUVs at 25 min in a desiccator. The Gaussian fit of 4 trials is shown in Figure 5.6 depicts the overall mean of Gaussian curves. Table 5.5 explains the percentage of GUVs under 30 µm and above 30 µm. As it is clear from the table that the population of GUVs less than 30 um is around 76%.

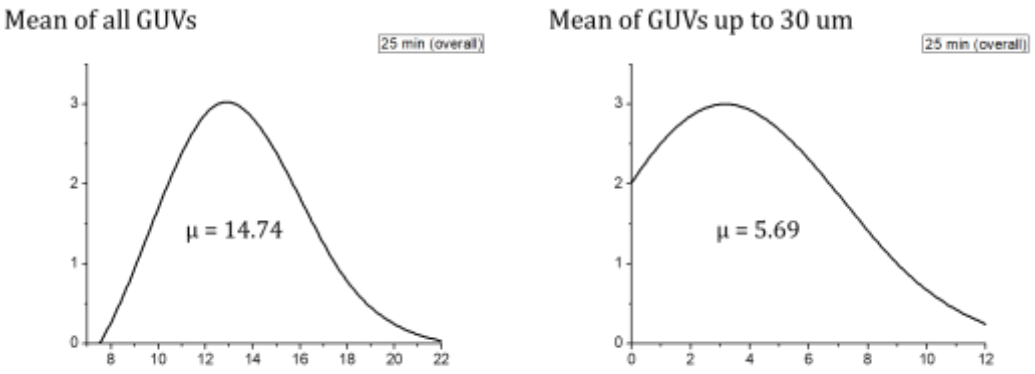

Figure 5.6 Comparison between the mean value of all size of GUVs and GUVs under the 30-um generated after keeping for 25 minutes in a desiccator

Table 5.5 The table shows the percentage of GUVs under and above 30-um generated after keeping for 25 minutes in a desiccator

Trials	0-30	>30
25 min 1	80.00%	20.00%
25 min 2	81.42%	18.57%
25 min 3	72.85%	27.14%
25 min 4	70.00%	30.00%
Average	76.07%	23.93%

Figure 5.7 represents the size distribution of the produced GUVs at 30 min in a desiccator. The Gaussian fit of 4 trials is shown in Figure 5.7 depicts the overall mean of Gaussian curves. Table 5.6 explains the percentage of GUVs under 30 μm and above 30 μm. As it is clear from the table that the population of GUVs less than 30 um is around 85%. So, most of the generated GUVs were smaller in size.

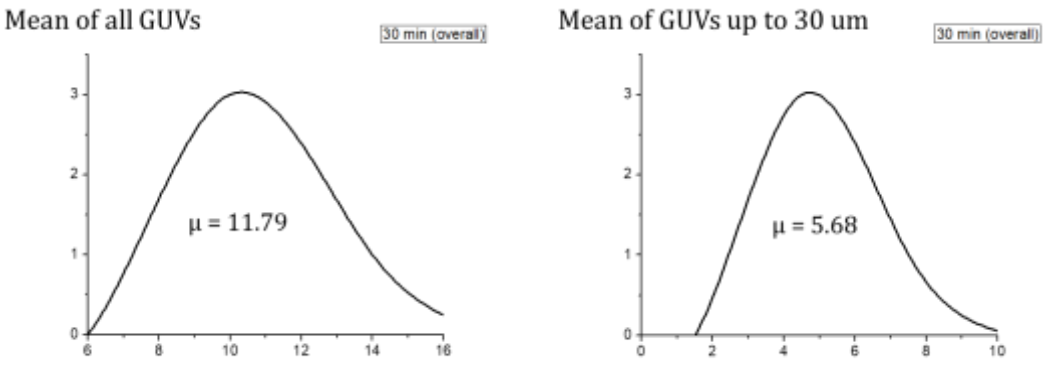

Figure 5.7 Comparison between the mean value of all size of GUVs and GUVs under the 30-um generated after keeping for 30 minutes in a desiccator

Table 5.6 The table shows the percentage of GUVs under and above 30-um generated after keeping for 30 minutes in a desiccator

Trials	<30	>30
30 min 1	78.57%	21.42%
30 min 2	81.42%	18.57%
30 min 3	94.28%	5.71%
30 min 4	87.14%	12.85%
Average	85.35%	14.64%

5.2 Permeability Testing

In this section and subsections, the results obtained from off-chip and on-chip measurements are discussed in detail.

5.3 Off-Chip Passive Permeability Testing

As mentioned in chapter 4, the impedance change on a frequency range reveals the impedance value at a particular frequency as shown in Figure 5.8. For instance, at 100 KHz, the impedance value is above 2 Kohm. This value was considered a reference value to compare off-chip and on-chip experiments. The LCR meter which was used for conducting experiments is up to 200 KHz and can provide 1.5 V maximum.

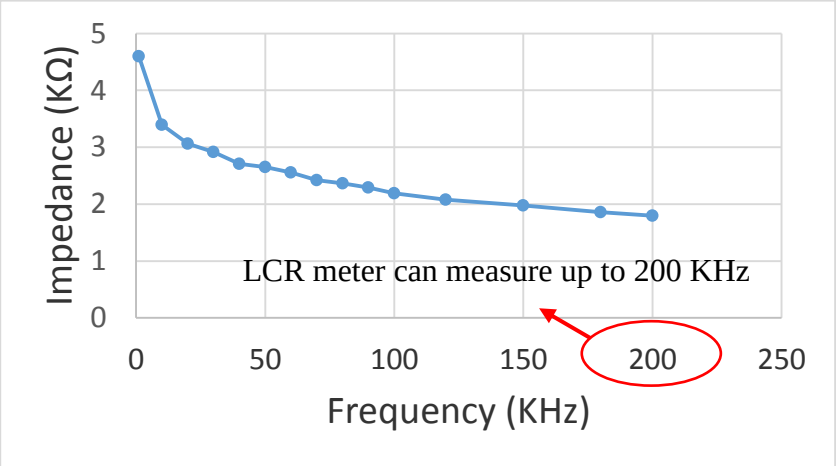

Figure 5.8 Impedance measurement with respect to the frequency range

5.3.1 Conductivity Measurements

Figure 5.9 displays the variation in conductivity for NF (pH-9, 7, 5) loaded GUVs over time. It is inferred that the conductivity for NF pH-5 and pH-7 in GUVs is not varying much, the values are around 800 and 900 uS/cm^2 respectively. However, the conductivity for NF (pH-9) loaded GUVs is around 50 uS/cm^2. There is no abrupt change in the conductivity which can represent the relation of permeability of antibiotic through GUVs. So, impedance measurements have been performed to monitor the behaviour of antibiotic as electrical circuit of vesicle membrane represent impedance.

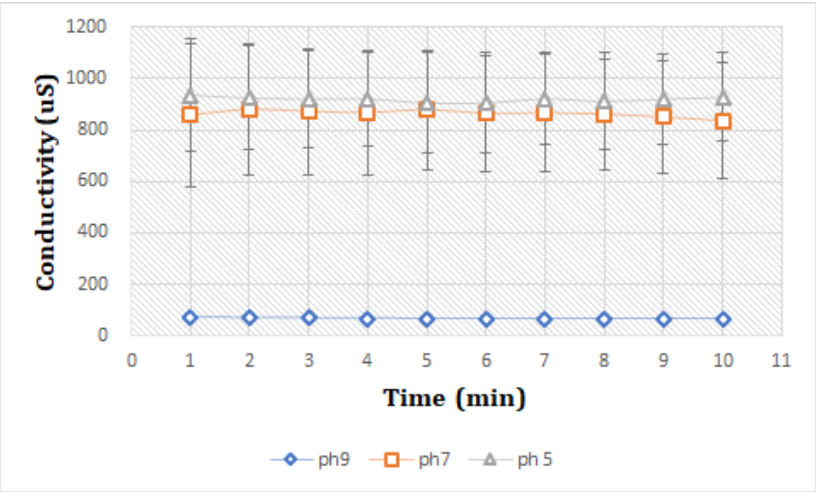

Figure 5.9 conductivity versus time

5.3.2 Impedance Measurements

The results indicate that the NF concentration decreases in the suspending medium. It is assumed that the NF of pH 9 has greater permeation to the GUVs as followed by NF of pH 7 and the NF of pH-5. The assumption is taken from a publication authored by Cama et al (J Cama et al., 2014). They determined that the permeability coefficient of the antibiotic norfloxacin across DPhPC lipid membranes at pH 7, validated the predictions for the effect of pH on norfloxacin permeability. The impedance and admittance values are decreasing and increasing from 21 to 16 Kohm and from 49 to 69 uS respectively. The graphs are shown in Figure 5.10. The error bars are standard deviation.

There is 5 % , 10% amd 19 % decrease in the impedance value at ph 9, 7 and 5 respectively. The percentage was calculated by using equation 5.1:

$$Permeability\ rate = \frac{Z10-Z1}{Z10} * 100 \qquad \textbf{(5.1)}$$

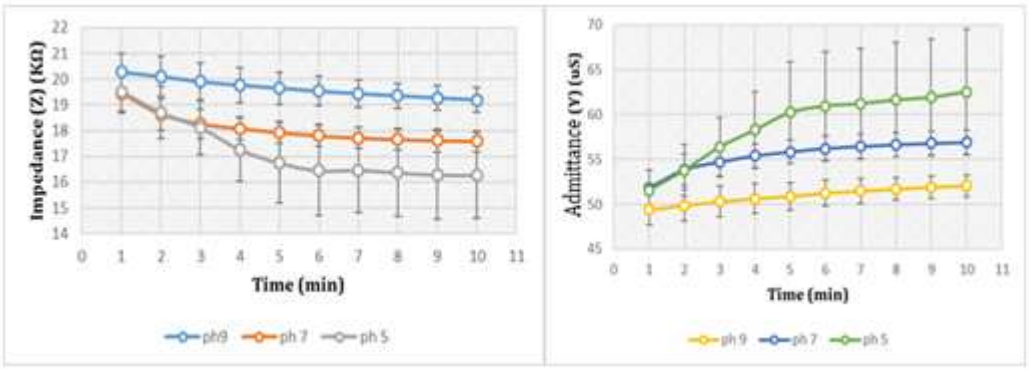

Figure 5.10 Impedance and admittance shifts over time of NF loaded GUVs

5.4 Off-Chip Active Permeability Testing

The bulk testing was carried out to check conductivity with conductivity meter and impedance measurement with LCR meter. GUVs were loaded with OmpF porin purified from E. Coli.

5.4.1 Conductivity Measurements

Figure 5.11 displays the variation in conductivity at NF (pH-9,7,5) loaded pro-GUVs over time. As compared to Figure 5.9 conductivity at NF pH-5 and pH-9 in GUVs is not varying much, the values are around 20 and 50 uS/cm^2 respectively. However, the conductivity for NF (pH-7) loaded pro-GUVs is around 450 uS/cm^2. Even with protein embedded GUVs, the change in the conductivity is not showing much information about permeability of antibiotic. So, impedance measurements have been done to monitor the behaviour of antibiotic as electrical circuit of vesicle membrane represents impedance.

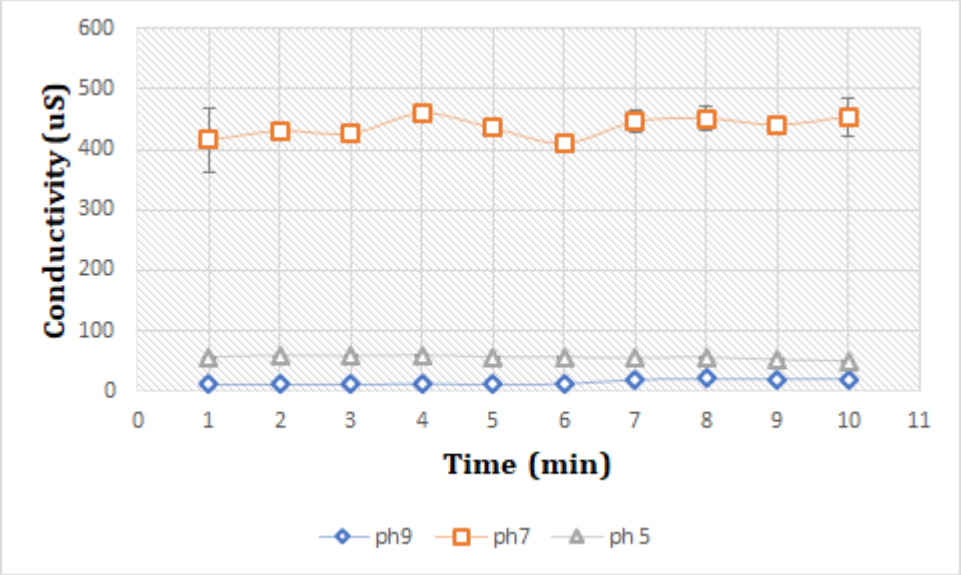

Figure 5.11 Conductivity versus time

5.4.2 Impedance Measurements

The NF concentration dropped in the suspending medium at a slow rate. The impedance obtained using pro-GUVs was small. It is envisioned that pro-GUVs uptook NF faster than protein-free GUVs. That is why the shift in impedance (Figure 5.12) is small (just 1 Kohm and 1 mS) in contrast to Figure 5.12. It is presumed that the NF of pH 7 has greater permeation to the GUVs as followed by NF of pH 5 and the NF of pH 9. The assumption is taken from a publication authored by Cama et al (J Cama et al., 2014).

15%, 45%and 29 % drop was observed in case of pro-GUVs at pH 9,7 and 5 respectively. These values were much higher than the decrease shown in case of GUVs. Thus, the permeation rate of NF through pro-GUVs was 10 times faster than GUVs.

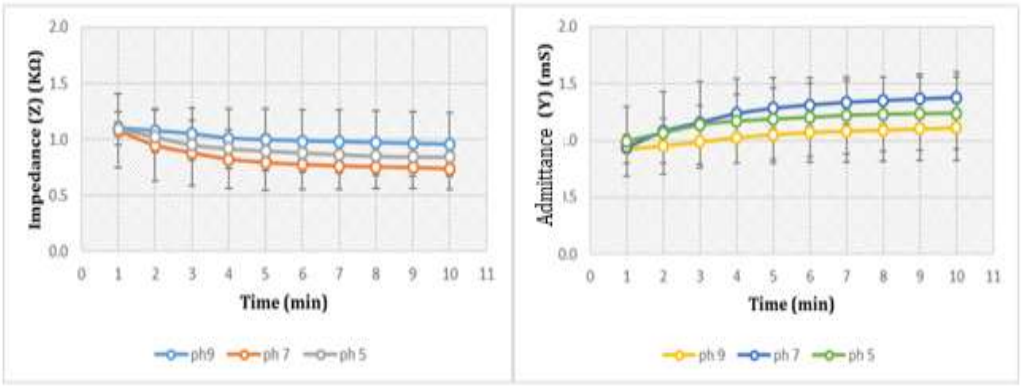

Figure 5.12 Impedance and admittance shifts over time of NF loaded pro-GUVs

5.5 Comparison of Off-chip Passive and Active Permeability Testing

Figure 5.13, Figure 5.14 and Figure 5.15 presents the comparison between the impedance and admittance shift of NF (pH-5,7,9) loaded GUVs and pro-GUVs. It is obvious that the active permeability is quite higher than the passive permeability. The impedance is around 20 Kohm and 1 Kohm for NF loaded GUVs and pro-GUVs respectively. The admittance is around 50 uS and 1 mS for NF loaded GUVs and pro-GUVs respectively. Each experiment was conducted 4 times to verify the results. An abrupt shift in the impedance values clears the permeation rate of pro-GUVs is 10 times more than GUVs.

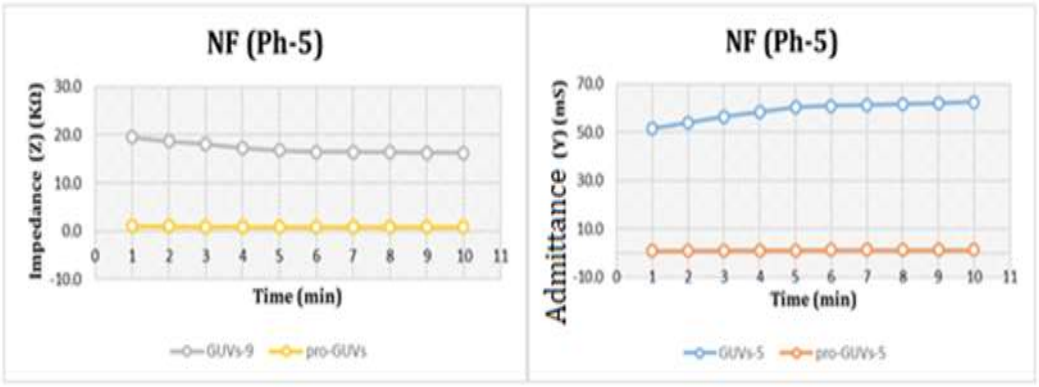

Figure 5.13 The comparison between the impedance and admittance shift of NF (pH-5) loaded GUVs and pro-GUVs

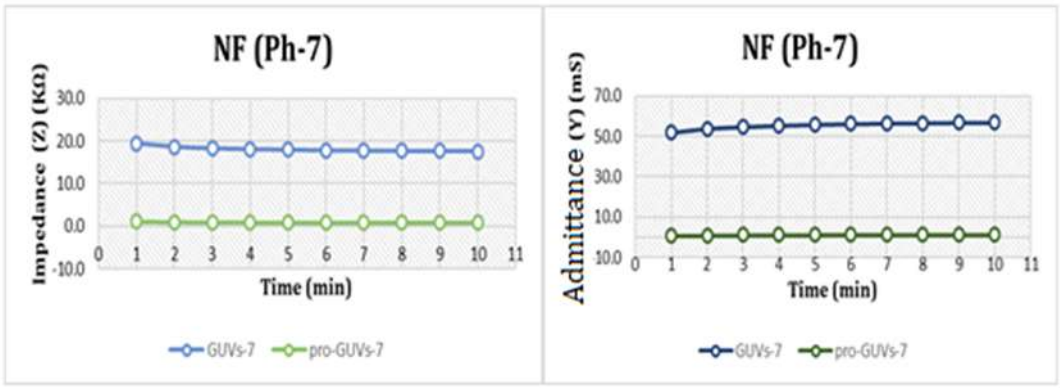

Figure 5.14 The comparison between the impedance and admittance shift of NF (pH-7) loaded GUVs and pro-GUVs

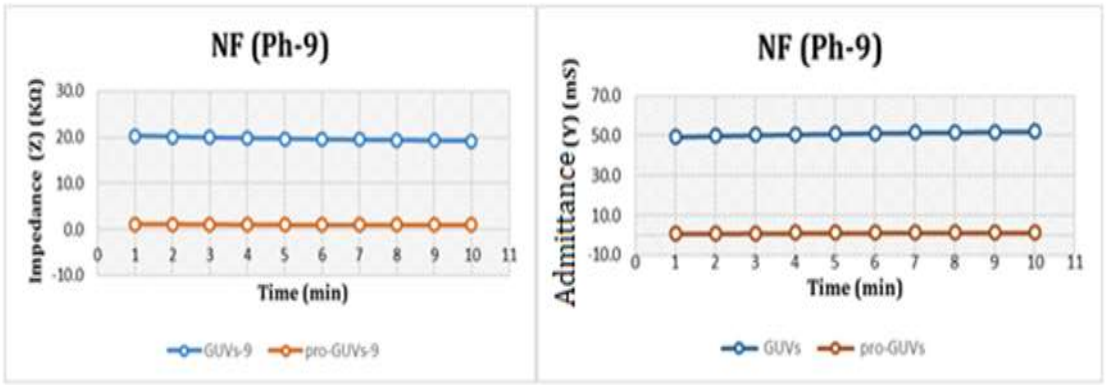

Figure 5.15 The comparison between the impedance and admittance shift of NF (pH-9) loaded GUVs and pro-GUVs

5.6 On-chip Passive Permeability Testing

The on-chip analysis was conducted with the same equipment as mentioned in chapter 4. Four trials were performed to validate the results.

5.6.1 Impedance Measurements

The results obtained indicate the NF concentration has not a significant increment or decrement when uptaken by GUVs. It is assumed that the NF of pH 7 has greater permeation to the GUVs as compared to NF of pH 9 and the NF of pH-5. The assumption is taken from a publication authored by Cama et al [9]. They determined that the permeability coefficient of the antibiotic norfloxacin across DPhPC lipid membranes at pH 7, and validated the predictions for the effect of pH on norfloxacin permeability. Because molecules of NF of pH-7 do not ionized in contrast to NF of pH-9 and 5. So, there is no effect on the impedance measurements. The impedance and admittance values are around 1.5 to 2.5 Mohm and from 0.5 to 0.6 uS respectively. The graphs are shown in Figure 5.16.

There is 11 % , 7% and 17 % decrease in the impedance value at ph 9, 7 and 5 respectively. The percentage was calculated by using equation 5.1.

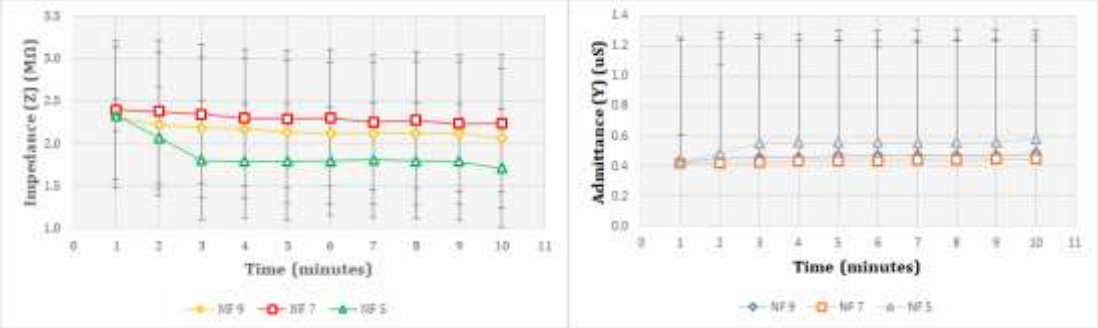

Figure 5.16 Impedance and admittance shifts over time of NF loaded GUVs

5.7 On-chip active permeability testing

The on-chip testing was carried out to determine the permeability rates through porins using Chip 2.

5.7.1 Impedance Measurements

As the NF concentration drops in the suspending medium, the impedance value shows a decreasing trend. The trend observed for impedance of pro-GUVs is very clear and shows that pro-GUVs uptook NF faster than protein-free GUVs. That is why the impedance value as shown in Figure 5.12 dropped from 0.9 or 1 Mohm to 0.7 Mohm which slighly lower than the impedance value of passive permeation. It is seen in Figure 5.17 that the NF of pH 7 has greater permeation to the GUVs as followed by NF of pH 5 and the NF of pH 9.

31%, 34%and 36% drop was observed in case of pro-GUVs at pH 9,7 and 5 respectively. These values were much higher than the decrease shown in case of GUVs. Thus, the permeation rate of NF through pro-GUVs was 20 folds faster than GUVs for on-chip experiments.

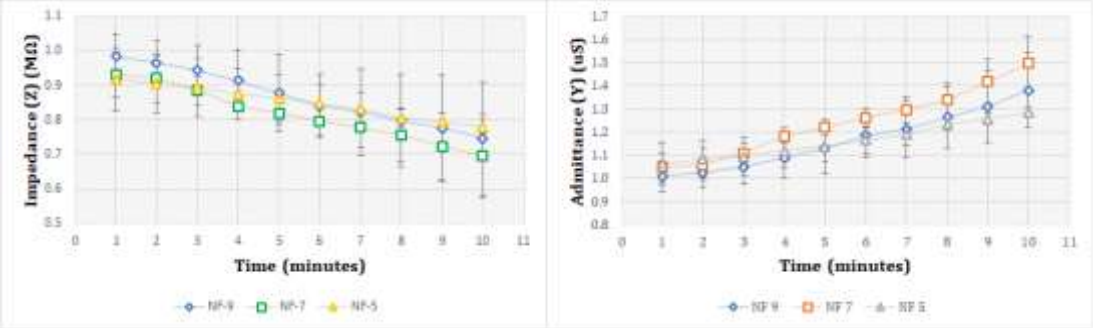

Figure 5.17 Impedance and admittance shifts over time of NF loaded pro-GUVs

5.8 Comparison of On-chip Passive and Active Permeability Testing

Figure 5.18, Figure 5.19 and Figure 5.20 explain the comparison between the impedance and admittance shift of NF (pH-5, 7, 9) loaded GUVs and pro-GUVs. Not much but 1 Mohm shift in impedance value vividly determne the permeability of NF 9 inside pro-GUVs greater than the permeability of NF 9 inside GUVs. The impedance is around 2.2 Mohm and 1 Mohm for NF 9 loaded GUVs and pro-GUVs respectively. The admittance is around 0.4 uS and 1.3 uS for NF 9 loaded GUVs and pro-GUVs respectively. Each experiment was conducted 4 times to verify the results.

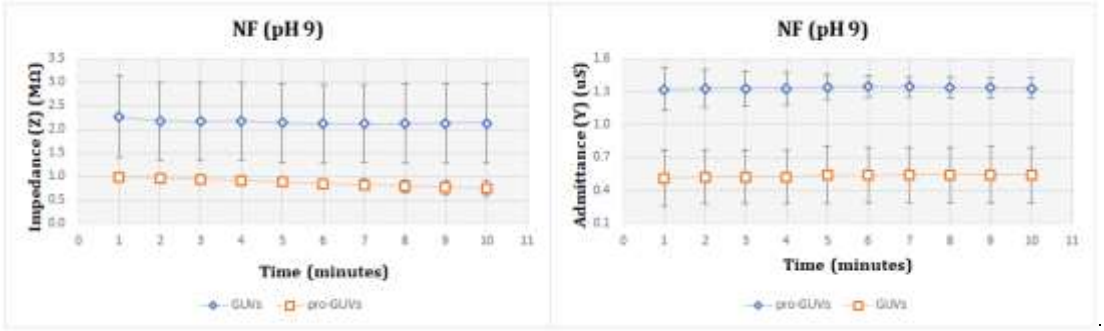

Figure 5.18 The comparison between the impedance and admittance shift of NF (pH-5) loaded GUVs and pro-GUVs

The impedance is around 2.2 Mohm and 1 Mohm for NF 7 loaded GUVs and pro-GUVs respectively. The impedance value for pro-GUVs decreased to 0.6 Mohm. The admittance is around 0.4 uS and 1.0 uS for NF 7 loaded GUVs and pro-GUVs respectively. The admittance value for pro-GUVs inreased to 1.2 uS.

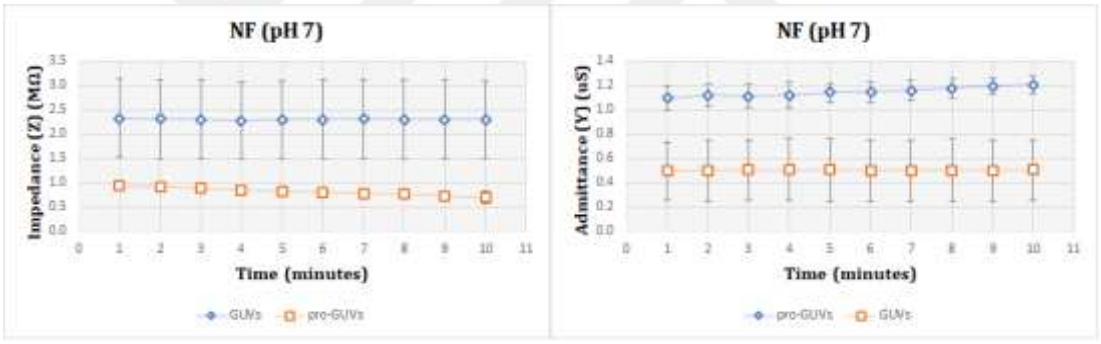

Figure 5.19 The comparison between the impedance and admittance shift of NF (pH-7) loaded GUVs and pro-GUVs

The impedance is around 1.7 Mohm and 1 Mohm for NF 5 loaded GUVs and pro-GUVs respectively. The impedance value for pro-GUVs decreased to 0.8 Mohm but increased for GUVs to 2.0 Mohm after 10 minutes. The admittance is around 1.2 uS and 0.6 uS after 1 minute for NF 7 loaded GUVs and pro-GUVs respectively. Eventually, after 10 minutes, the admittance value for pro-GUVs decreased to 1.1 uS and 0.3 uS for GUVs.

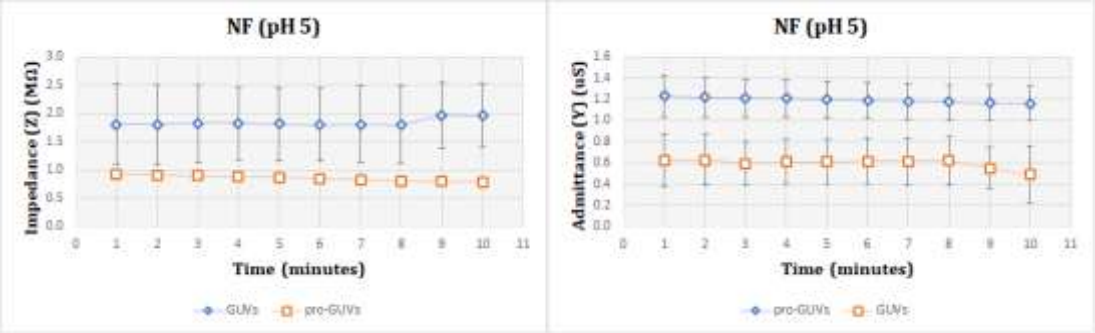

Figure 5.20 The comparison between the impedance and admittance shift of NF (pH-9) loaded GUVs and pro-GUVs

5.9 Discussion

The GUVs produced by electroformation has been studied by changing evaporation time. The Gaussian distribution analysis shows that the majority of the vesicles is under 30 um in size.

To understand the diffusion through the membrane of vesicles, the conductivity and impedance were measured. The outer membrane of GUVs consists of RC circuit (Figure 5.21). The lipid bilayer acts like an insulator separating two conducting media: the external medium and the internal medium. This geometry constitutes an electric capacitor where the two conducting plates are the ionic media and the membrane is the dielectric. The capacitance c of a capacitor increases with the area of the plates and decreases with the separation between the plates according to the the relation

$$c = \varepsilon \frac{A}{d} \quad \textbf{(5.2)}$$

where A is the membrane area, d is the separation between the plates or the membrane thickness and ε is the dielectric constant. In the case of the membrane, it is more convenient to define the capacitance as independent of the amount of area involved and specify as Cm which is defined as the capacitance per unit area or c/A.

$$Cm = \frac{\varepsilon}{d} \quad \textbf{(5.3)}$$

As the thickness d is only 25 Å, the specific capacitance of the membrane is very high, close to 1 μF/cm^2. Having the properties of a capacitor, the membrane is able to separate electric charge, achieved by a difference in the number of anions and cations

on each side of the membrane; this charge separation in turn produces a potential difference across the membrane. In a capacitor the potential difference V is related to the charge Q by

$$Q = CV \tag{5.4}$$

where C is the capacitance. It is important to notice that in the case of the lipid membrane a small amount of charge separation is able to generate a large potential difference. The energy to put an ion or a molecule into the lipid bilayer is so large that the membrane to be practically impermeable to ions would be expected. But it is possible with the help of the Nernst Potential which simplifies the latter problem by expressing the net ion flow j in terms of the chemical and electrical gradients.

$$j = -D[\frac{dC}{dx} + C\left(\frac{zF}{RT}\right)\frac{dV}{dx} \tag{5.5}$$

where D is the diffusion coefficient, C is the concentration, R is the gas constant, V is the voltage, z is the valence, F is the Faraday constant, and T is the temperature. When j=0 (no net flow), eq (11) can be integrated and give:

$$V = \frac{RT}{zF}\ln\frac{Co}{Ci} \tag{5.6}$$

which is the Nernst equation that relates the voltage V across the membrane which is in equilibrium with the concentration gradient established by the concentrations Co, outside, and Ci, inside. In simple words, the resistance of the membrane is constant but the capacitance of membrane varies. The impedance of the basic RC circuit is

$$Z = \frac{RXc}{\sqrt{R^2+Xc^2}} = \frac{V}{I} \tag{5.7}$$

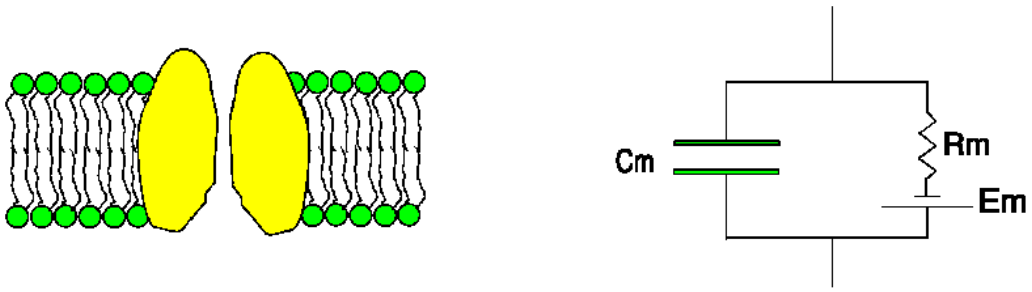

Figure 5.21 Electric model of membrane

Where Z is impedance, R is resistance, Xc is frequency dependent capacitance, V is voltage and I is current. So, from equation 5.6 and 5.7, Co (outside) and Ci (inside) concentartion of norfloxacin molecules can be correlated with the impedance. It is observed from the equation 5.6 and 5.7 that impedance is directly proportional to the concentration.

$$\frac{IRXc}{\sqrt{R^2+Xc^2}} = \frac{RT}{zF}\ln\frac{Co}{Ci} \quad \textbf{(5.8)}$$

The current through the conductive part of the membrane can be expressed as a product of a conductance and a driving force:

$$I = g(V - Ee) \quad \textbf{(5.9)}$$

where V-Ee is the driving force and g is the conductance (reciprocal value of resistance, R=1/g) expressed in Siemens(S=1/ohm). V is the membrane potential and Ee is the reversal potential [40]. The current remains constant. In short, the ratio of outside concentration to inside concentration can be determined with the impedance value measured from equation 5.8.

$$Impedance \propto \frac{outside\ concentration}{inside\ concentration} \quad (\mathbf{5.10})$$

It is evident from equation 5.10 that if the impedance at particular pH decreases then concentration inside the vesicle increases and vice versa. The results shown in above section represent the decrement in impedance value which shows the increament of NF molecules inside the vesicles.

The impedance measurement was performed using two different chip designs. For the fabrication of chip, chip 1 was produced without microfluidic channel and was used for off-chip testing. Chip 2 design is the result of the best of other designs based on specific parameters such as antibiotic uptake time, electrodes placement for measurements and likewise. The diffusion of NF into GUVs was on the order of minutes at pH-5, 7 and 9. Moreover, the flow rate, 0.5 ul/min was used for the microfluidics system, was assumed to be optimum. In the chip 2 microfluidic channel, the giant unilamellar vesicles took around 7 minutes to travel and so as the Norfloxacin. At the optimum flow rate, the experiments indicated that the NF was uptaken by GUVs across the whole channel starting from the first T junction. There were total 6 junctions

at which impedance was measured to ensure the change in the permeability of NF over time. The conductivity was also tested for off-chip experiments with a conductivity meter and considered as same for on-chip experiments. The impedance and admittance were measured at 6 junctions (shown in Figure 3.3) in the chip with the help of electrode array assigned at junctions. The electrodes were placed underneath the channel to calculate the impedance value with respect to time. The significant shift observed in the measured impedance and admittance data can be related to the permeability of NF through vesicles. The data is shown for the length traveled, L=360 mm.

From the graphs explained above, the impedance at pH 9 is higher than that recorded at pH 7 and 5 but pH 7 is highly considerable in contrast to pH 5 and 9. According to literature, the molecules of NF pH 7 remain uncharged whereas, at pH 5 and 9, the NF molecules become zwitterions [8]. At pH 5, the NF breaks with the majority of positively charged ions, pH 7 remains unionized and ions of NF pH 9 becomes negatively charged (assumption). So at pH 5, fewer NF molecules permeate the membrane. In addition, the comparison graphs determine the permeability of NF over time by considering the RC circuit of the membrane of vesicles.

In conclusion, the permeation of antibiotic thorough vesicle has been studied. The vesicles generated by electroformation mimic the cell membrane of a living cell and the he impedance measurements represent a way to determine the permeability rates over time. This label-free device is simple which is fabricated by standard fabrication technique and can be used for different studies whether the drug is autofluorescent or non-autofluorescent.

CHAPTER 6

CONCLUSION

In this project, a microfluidic chip made up of PDMS-based microfluidic channels and a titanium electrode array was produced using standard lithography techniques and integrated to constitute a hybrid on-chip permeability device. As a proof-of-concept, the hybrid device was then used for the passive and active permeability testing using impedance and admittance measurements.

PDMS based microfluidic chips were preferred due to their ease of use, fast production, and quick response. Experimental results show that integrated microfluidic chips were effective in understanding the permeability rates using conductivity and impedance shifts with respect to concentrations in and out of the vesicles over time. In particular, it is observed that the uptake of NF (pH-7) by GUVs is considerable because the molecules of NF donot ionized. Whereas, the NF molecules at pH 5 and 9 get ionized and may result in the error in the measurements.

Further studies will focus on introducing the optimum intrinsic and extrinsic conductivity and permittivity of GUVs and a crossover frequency. This technique will be used for calculating the physical/electrical properties of the cell membrane and the antibiotic concentration measurement by DEP. This will then improve our knowledge on the permeability rates.

REFERENCES

[1] 3D structure for Norfloxacin (DB01059) - DrugBank. (n.d.). Retrieved June 15, 2019, from https://www.drugbank.ca/structures/small_molecule_drugs/DB01059.

[2] Abd Rahman, N., Ibrahim, F., & Yafouz, B.. Dielectrophoresis for Biomedical Sciences Applications: A Review. Sensors (Basel, Switzerland), 17(3), 2017. https://doi.org/10.3390/s17030449.

[3] Batchelor, G. (n.d.). An introduction to fluid dynamics. (C. M. Library, Ed.) ((2nd ed)). Cambridge University Press.

[4] Bhalla, N., Jolly, P., Formisano, N., & Estrela, P.. Introduction to biosensors. Essays in Biochemistry, 60(1), 1–8, 2016. https://doi.org/10.1042/EBC20150001.

[5] Breton, M., Amirkavei, M., & Mir, L. M. Optimization of the Electroformation of Giant Unilamellar Vesicles (GUVs) with Unsaturated Phospholipids. The Journal of Membrane Biology, 248(5), 827–835, 2015a. https://doi.org/10.1007/s00232-015-9828-3.

[6] Breton, M., Amirkavei, M., & Mir, L. M. Optimization of the Electroformation of Giant Unilamellar Vesicles (GUVs) with Unsaturated Phospholipids. Journal of Membrane Biology, 2015b. https://doi.org/10.1007/s00232-015-9828-3.

[7] Cama, J., Chimerel, C., Pagliara, S., Javer, A., & Keyser, U. F.. A label-free microfluidic assay to quantitatively study antibiotic diffusion through lipid membranes. Lab on a Chip, 2014a. https://doi.org/10.1039/c4lc00217b.

[8] Cama, J., Chimerel, C., Pagliara, S., Javer, A., & Keyser, U. F.. A label-free microfluidic assay to quantitatively study antibiotic diffusion through lipid membranes. Lab Chip, 14(13), 2303–2308, 2014b. https://doi.org/10.1039/C4LC00217B.

[9] Cama, J, Javer, A., & Keyser, U. F. Lab on a Chip study antibiotic diffusion through lipid membranes , 2303–2308, 2014. https://doi.org/10.1039/c4lc00217b.

[10] Cama, Jehangir, Bajaj, H., Pagliara, S., Maier, T., Braun, Y., Winterhalter, M., & Keyser, U. F. Quantification of Fluoroquinolone Uptake through the Outer Membrane Channel OmpF of Escherichia coli. Journal of the American Chemical Society, 137(43), 13836–13843, 2015a. https://doi.org/10.1021/jacs.5b08960.

[11] Cama, Jehangir, Bajaj, H., Pagliara, S., Maier, T., Braun, Y., Winterhalter, M., & Keyser, U. F.. Quantification of Fluoroquinolone Uptake through the Outer Membrane Channel OmpF of Escherichia coli. Journal of the American Chemical Society, 137(43), 13836–13843, 2015b. https://doi.org/10.1021/jacs.5b08960.

[12] Casquillas, V., Houssin, T., & Durieux, L.. Microfluidics and microfluidic

devices: a review. Elveflow, 1–9, 2015.

[13] Castellanos, A., Ramos, A., Gonzales A., Green, N.G., and Morgan, H. (n.d.). Electrodynamics and Dielectrophoresis in Microsystems: Scaling Laws, in Journal of Physics 2584–2597. Applied Physics.

[14] Çetin, B., & Li, D. Dielectrophoresis in microfluidics technology. Electrophoresis, 32(18), 2410–2427, 2011. https://doi.org/10.1002/elps.201100167.

[15] Díaz, R., & Payen, S. (n.d.). Biological cell separation using dielectrophoresis in a microfluidic device, 1–4.

[16] Fernandez, R. E., Rohani, A., Farmehini, V., & Swami, N. S.. Review: Microbial analysis in dielectrophoretic microfluidic systems. Analytica Chimica Acta, 966, 11–33, 2017. https://doi.org/10.1016/j.aca.2017.02.024.

[17] Green, N. G., & Morgan, H.. Dielectrophoretic separation of nano-particles. Journal of Physics D: Applied Physics, 30(11), L41–L44, 1997. https://doi.org/10.1088/0022-3727/30/11/001.

[18] Gupta, S., Ramesh, K., Ahmed, S., & Kakkar, V.. Lab-on-chip technology: A review on design trends and future scope in biomedical applications. International Journal of Bio-Science and Bio-Technology, 8(5), 311–322, 2016. https://doi.org/10.14257/ijbsbt.2016.8.5.28.

[19] Hughes, M. P., Morgan, H., & Rixon, F. J.. Measuring the dielectric properties of herpes simplex virus type 1 virions with dielectrophoresis. Biochimica et Biophysica Acta (BBA) - General Subjects, 1571(1), 1–8, 2002. https://doi.org/10.1016/S0304-4165(02)00161-7.

[20] Jones, T. B. (Thomas B.. Electromechanics of particles. Cambridge University Press 1995.

[21] Judy, J. W.. Microelectromechanical systems (MEMS): fabrication, design and applications. Smart Materials and Structures, 10(6), 1115–1134, 2001. https://doi.org/10.1088/0964-1726/10/6/301.

[22] Li, C. Introduction and Overview of Biosensors and Electrochemistry. Powerpoint Presentation, 1–31, 2007. Retrieved from papers://80ebdcbb-5aec-43b3-98b5-dad4eae31b2e/Paper/p3060.

[23] Luka, G., Ahmadi, A., Najjaran, H., Alocilja, E., Derosa, M., Wolthers, K., … Hoorfar, M.. Microfluidics Integrated Biosensors : A Leading Technology towards Lab-on-a-Chip and Sensing Applications, 30011–30031, 2015. https://doi.org/10.3390/s151229783.

[24] Markx, G. H., Rousselet, J., & Pethig, R.. DEP-FFF: Field-Flow Fractionation Using Non-Uniform Electric Fields. Journal of Liquid Chromatography & Related Technologies, 20(16–17), 2857–2872, 1997.

https://doi.org/10.1080/10826079708005597.

[25] Microfluidics? A general overview. (n.d.). Retrieved July 4, 2019, from https://www.elveflow.com/microfluidic-tutorials/microfluidic-reviews-and-tutorials/microfluidics/

[26] Mikkelsen, A., Kertmen, A., & Khobaib, K.. Assembly of 1D Granular Structures from Sulfonated Polystyrene Microparticles, June 2018. https://doi.org/10.3390/ma10101212.

[27] Odou, M. F., Singer, E., Romond, M. B., & Dubreuil, L.. Isolation and characterization of a porin-like protein of 45 kilodaltons from Bacteroides fragilis, 166, 1998.

[28] PARTICLE SEPARATION IN MICROFLUIDIC SYSTEMS USING AC. June, 2015.

[29] Pereno, V., Carugo, D., Bau, L., Sezgin, E., Bernardino de la Serna, J., Eggeling, C., & Stride, E.. Electroformation of Giant Unilamellar Vesicles on Stainless Steel Electrodes. ACS Omega, 2(3), 994–1002, 2017. https://doi.org/10.1021/acsomega.6b00395.

[30] Purushothaman, S., Cama, J., & Keyser, U. F. Dependence of norfloxacin diffusion across bilayers on lipid composition. Soft Matter, 12(7), 2135–2144, 2016. https://doi.org/10.1039/C5SM02371H.

[31] Rao Karumuri, S., Girija Sravani, K., Durga Sailaja, S., Sekhar, J. V., Srinivas, Y., & Bhattacharjee, R. (n.d.). Micro-Electro-Mechanical-Systems (MEMS) Technology. Scholars Research Library Archives of Applied Science Research, Vol. 2012. Retrieved from www.scholarsresearchlibrary.com.

[32] Rideau, E., Dimova, R., Schwille, P., Wurm, F. R., & Landfester, K.. Liposomes and polymersomes: a comparative review towards cell mimicking. Chemical Society Reviews, 47(23), 8572–8610, 2018. https://doi.org/10.1039/C8CS00162F.

[33] Safavieh, M., Pandya, H. J., Venkataraman, M., Thirumalaraju, P., Kanakasabapathy, M. K., Singh, A., Shafiee, H. Rapid Real-Time Antimicrobial Susceptibility Testing with Electrical Sensing on Plastic Microchips with Printed Electrodes. ACS Applied Materials and Interfaces, 9(14), 12832–12840, 2017. https://doi.org/10.1021/acsami.6b16571.

[34] Schaich, M., Cama, J., Al Nahas, K., Sobota, D., Jahnke, K., Deshpande, S., Keyser, U. F. (n.d.). An integrated microfluidic platform for quantifying drug permeation across biomimetic vesicle membranes. https://doi.org/10.1101/523431.

[35] Schmid, E. M., Richmond, D. L., & Fletcher, D. A.. Reconstitution of proteins on electroformed giant unilamellar vesicles. Methods in Cell Biology, 128, 319–338, 2015. https://doi.org/10.1016/BS.MCB.2015.02.004.

[36] Sensor, M. M.. MEMS Technology in Biomedical Sensor Application MEMS Technology in Biomedical Sensor Application. System, 2002.

[37] Soeraasen, O., & Ramstad, J. E.. From MEMS devices to smart integrated systems. Microsystem Technologies, 14(7), 895–901, 2008. https://doi.org/10.1007/s00542-007-0523-x.

[38] Soheila ZEINALI. Microfluidic Device With 3D Electrode Structure for High Throughput Dielectrophoretic Applications, 2014.

[39] The Difference Between Passive and Active Transport : active, bioogy, cell, cellular, en, energy, passive, science, transport | Glogster EDU - Interactive multimedia posters. (n.d.). Retrieved July 25, 2019, from https://edu.glogster.com/glog/the-difference-between-passive-and-active-transport/1ln5phdc4ln?=glogpedia-source.

[40] The nerve impulse. (n.d.). Retrieved from http://nerve.bsd.uchicago.edu/TheNerveImpulse05.pdf.

[41] Trabzon, L. PRODUCING, DESIGNING AND CHARACTERISING POLYMER BASED MICROFLUIDIC SYSTEM TO SEPERATE MICRO-PARTICLE, 2012.

[42] Varadan, V. K., & Varadan, V. V.. Microsensors, microelectromechanical systems (MEMS), and electronics for smart structures and systems. Smart Materials and Structures, 9(6), 953–972, 2000. https://doi.org/10.1088/0964-1726/9/6/327.

[43] Yole Développement MEMS compound semiconductors advanced packaging PV photovoltaic 3D-IC LED optoelectronics power electronics microfluidic technology market research and strategy report analysis - REPORTS. (n.d.). Retrieved April 28, 2019, from http://www.yole.fr/Reports.aspx.

CURRICULUM VITAE



PERSONAL INFORMATION

Name Surname	**:**	JASPREET KAUR
Date of Birth	**:**	28/01/1990
Phone	**:**	905522171796
E-mail	**:**	jk28jan@gmail.com

EDUCATION

High School	**:**	S.G.R.D. SEN SEC SCHOOL, INDIA (2006-2007)
Bachelor	**:**	PUNJAB TECHNICAL UNIVERSITY, INDIA (2007-2011)
Master's degree	**:**	ANKARA YILDIRIM BEYAZIT UNIVERSITY, TURKEY (2017-2019)

WORK EXPERIENCE

PROJECT FELLOW : CSIR-CEERI, PILANI, INDIA

TOPICS OF INTEREST

- ELECTRONICS
- NANOTECHNOLOGY
- SENSORS

